Discreteness-Aware Approximate Message Passing for Discrete-Valued Vector Reconstruction

Ryo Hayakawa, *Student Member, IEEE*, and Kazunori Hayashi, *Member, IEEE*

***Abstract*—This paper considers the reconstruction of a discrete-valued random vector from possibly underdetermined linear measurements using sum-of-absolute-value (SOAV) optimization. The proposed algorithm, referred to as discreteness-aware approximate message passing (DAMP), is based on the idea of approximate message passing (AMP), which has been originally proposed for compressed sensing. The DAMP algorithm has low computational complexity and its performance in the large system limit can be predicted analytically via state evolution framework, where we provide a condition for the exact reconstruction with DAMP in the noise-free case. From the analysis, we also propose a method to determine the parameters of the SOAV optimization. Moreover, based on the state evolution, we provide Bayes optimal DAMP, which has the minimum mean-square-error at each iteration of the algorithm. Simulation results show that the DAMP algorithms can reconstruct the discrete-valued vector from underdetermined linear measurements and the empirical performance agrees with our theoretical results in large-scale systems. When the problem size is not large enough, the SOAV optimization with the proposed parameters can achieve better performance than the DAMP algorithms for high signal-to-noise ratio.**

***Index Terms*—discrete-valued vector reconstruction, sum-of-absolute-value optimization, approximate message passing, state evolution.**

I. Introduction

In signal processing, it is an important problem to reconstruct a discrete-valued vector from its possibly underdetermined linear measurements. In communications systems, for example, multiuser detection [1]–[4], overloaded multiple-input multiple-output (MIMO) signal detection [5]–[7], and faster-than-Nyquist signaling [8], [9] can be regarded as such problems because the signals in digital communications are generally discrete-valued. The reconstruction of discrete-valued images can also be formulated similarly [10]. For such problems, the optimal maximum likelihood approach results in a combinatorial optimization problem and hence the computational complexity increases exponentially along the problem size. We thus require a low-complexity algorithm for the reconstruction, especially in large-scale problems.

Manuscript received April XX, 20XX; revised September XX, 20XX.

This work was supported in part by the Grants-in-Aid for Scientific Research no. 15K06064, 15H02252, 18K04148 and 18H03765 from the Ministry of Education, Culture, Sports, Science and Technology of Japan, and the Grant-in-Aid for JSPS Research Fellow no. 17J07055 from Japan Society for the Promotion of Science. This work has been partially presented in IEEE SPAWC 2017, Sapporo, Japan, July 3–6, 2017, and APSIPA ASC 2017, Kuala Lumpur, Malaysia, December 12–15, 2017.

Ryo Hayakawa is with Graduate School of Informatics, Kyoto University, Kyoto 606-8501, Japan (e-mail: rhayakawa@sys.i.kyoto-u.ac.jp).

Kazunori Hayashi is with the Graduate School of Engineering, Osaka City University, Osaka 558-8585, Japan (e-mail: kazunori@eng.osaka-cu.ac.jp).

Some methods based on convex optimization have been proposed for the large-scale discrete-valued vector reconstruction. The regularization-based method and the transform-based method [11] borrow the idea from compressed sensing [12], [13] in the formulation to obtain convex optimization problems. The optimization problems can be solved by interior point methods [14] as the standard linear programming. As for theoretical analysis, the required number of measurements in the large system limit has been derived for the binary vector reconstruction with the regularization-based method. A more general result has been obtained for the reconstruction of uniformly distributed discrete-valued vectors via the transform-based method. For non-uniformly distributed vectors, however, no analytical result has been provided. In [15], the box relaxation optimization has been proposed for the signal detection in code division multiple access (CDMA). Although the asymptotic performance of the method has been analyzed in [16], the analysis is limited to the reconstruction of uniformly distributed binary vector.

On the other hand, sum-of-absolute-value (SOAV) optimization has been proposed for the reconstruction of discrete-valued vector with any discrete distribution [17]. Although the SOAV optimization is similar to the regularization-based method, it can take the probability distribution of the unknown vector into consideration. They are actually equivalent when the unknown vector is uniformly distributed. The SOAV optimization is also convex, and efficient algorithms based on proximal splitting methods [18] have been proposed [4], [7]. Although some theoretical analyses have been provided for the optimization problem [4], [7], the required number of measurements for the reconstruction has not been obtained for the SOAV optimization.

In this paper, we propose an iterative algorithm based on the SOAV optimization problem, whose preliminary version has been presented in [19], [20]. By using the idea of the approximate message passing (AMP) algorithm [21], [22] for compressed sensing, we firstly consider a probability distribution corresponding to the SOAV optimization. We then approximate the sum-product belief propagation [23], [24] for the distribution and obtain the proposed algorithm, referred to as discreteness-aware AMP (DAMP). For the approximation in the derivation, we assume the large system limit, where the problem size increases to infinity with a fixed ratio of the number of measurements to the number of unknown variables. The DAMP algorithm has basically the same form as that of the original AMP algorithm for compressed sensing except for their soft thresholding functions. Hence, the order of the computational complexity is the same as that of

the original AMP algorithm. By using state evolution [21], [25], we analytically evaluate the asymptotic performance of the DAMP algorithm in the large system limit. We further derive the required number of measurements for the perfect reconstruction in the noise-free case. The analysis provides the optimal parameters of the soft thresholding function in terms of minimizing the required number of measurements. With the analytical result, we also propose a method to determine the parameters of the SOAV optimization. Moreover, on the basis of the state evolution, we derive Bayes optimal DAMP, which gives the minimum mean-square-error (MSE) at each iteration in the large system limit. Simulation results show that the proposed DAMP algorithms can reconstruct the discrete-valued vector from its underdetermined linear measurements. For large-scale problems, the performance agrees well with the theoretical result obtained with the state evolution. The SOAV optimization with the proposed parameters can achieve the better performance than that of the original SOAV optimization. Moreover, when the problem size is not large enough, it also outperforms some AMP-based algorithms in high signal-to-noise ratio (SNR) region. We also evaluate the performance when the measurement matrix is a partial discrete cosine transform (DCT) matrix. We compare the proposed methods with turbo compressed sensing [26], [27], which is a message passing-based algorithm designed for partial discrete Fourier transform (DFT) measurement matrices. For small-scale problems, Bayes optimal DAMP achieves better performance than turbo compressed sensing in the high SNR region.

One of major additional contributions from the conference versions [19], [20] is the extension of DAMP for any discrete distributions, while [19] and [20] consider only symmetric distributions and binary distributions, respectively. Moreover, we newly provide the optimization algorithm to determine the parameters of the soft thresholding function, which enables us to theoretically analyze the condition for the perfect reconstruction in some examples. Furthermore, we also propose a method to determine the parameters of the SOAV optimization, which will be shown to have better symbol error rate (SER) performance than the original optimization proposed in [17] in the simulations.

The rest of the paper is organized as follows: In Section II, we propose the DAMP algorithm for the discrete-valued vector reconstruction. Section III analyzes the performance of the DAMP algorithm via the state evolution framework and shows some examples of the analysis. We then apply the theoretical results to the SOAV optimization in Section IV and provide Bayes optimal DAMP in Section V. Section VI gives some simulation results, which demonstrate the performance of the proposed algorithms and show the validity of the theoretical analysis. Finally, we present some conclusions in Section VII.

In the rest of the paper, we use the following notations: we represent the transpose by $(\cdot)^{\mathrm{T}}$, the identity matrix by $\boldsymbol{I}$, the vector whose elements are all 1 by $\mathbf{1}$, and the vector whose elements are all 0 by $\mathbf{0}$. For a vector $\boldsymbol{u} = [u_1 \cdots u_N]^{\mathrm{T}} \in \mathbb{R}^N$, we define the ℓ_1 and ℓ_2 norms of $\boldsymbol{u}$ as $\|\boldsymbol{u}\|_1 = \sum_{n=1}^N |u_n|$ and $\|\boldsymbol{u}\|_2 = \sqrt{\sum_{n=1}^N u_n^2}$, respectively. We also define $\|\boldsymbol{u}\|_0$ as the number of nonzero elements in $\boldsymbol{u}$. $[\boldsymbol{u}]_n$ indicates the nth element of $\boldsymbol{u}$. We represent the sample mean of the elements of $\boldsymbol{u}$ by $\langle \boldsymbol{u} \rangle = \frac{1}{N}\sum_{n=1}^N u_n$. The matrix $\mathrm{diag}(u_1, \ldots, u_N) \in \mathbb{R}^{N\times N}$ denotes the diagonal matrix whose (n,n) element is u_n. For a function $h : \mathbb{R}^N \to \mathbb{R}$, the proximity operator [18] of h is defined as $\mathrm{prox}_h(\boldsymbol{u}) = \arg\min_{\boldsymbol{s}\in\mathbb{R}^N} \left\{ h(\boldsymbol{s}) + \frac{1}{2}\|\boldsymbol{s}-\boldsymbol{u}\|_2^2 \right\}$. We represent the sign function by $\mathrm{sgn}(\cdot)$. $\phi(z) = \frac{1}{\sqrt{2\pi}} \exp\left(-\frac{z^2}{2}\right)$ and $\Phi(z) = \int_{-\infty}^z \phi(z')\mathrm{d}z'$ are the probability density function and the cumulative distribution function of the standard Gaussian distribution, respectively.

II. Proposed Discreteness-aware AMP

In this section, we briefly explain the SOAV optimization [17] and propose DAMP by taking a similar approach to that of the AMP algorithm for compressed sensing [21].

A. SOAV Optimization

The SOAV optimization is a technique to reconstruct a discrete-valued vector such as $\boldsymbol{b} = [b_1 \cdots b_N]^{\mathrm{T}} \in \{r_1, \ldots, r_L\}^N \subset \mathbb{R}^N$ $(r_1 < \cdots < r_L)$ from its linear measurements

$$\boldsymbol{y} = \boldsymbol{A}\boldsymbol{b} + \boldsymbol{v}, \tag{1}$$

where $\boldsymbol{y} = [y_1 \cdots y_M]^{\mathrm{T}} \in \mathbb{R}^M$ and $\boldsymbol{A} \in \mathbb{R}^{M\times N}$. We denote the (m,n) element of $\boldsymbol{A}$ by $a_{m,n}$ $(m = 1, \ldots, M$ and $n = 1, \ldots, N)$. The vector $\boldsymbol{v}$ is an unknown additive Gaussian noise with mean $\mathbf{0}$ and covariance matrix $\sigma_v^2\boldsymbol{I}$. We assume that the elements of $\boldsymbol{b}$ are independent and identically distributed (i.i.d.) random variables from the known distribution $\Pr(b_n = r_\ell) = p_\ell$ $(n = 1, \ldots, N$ and $\ell = 1, \ldots, L)$. In this situation, $\boldsymbol{b} - r_\ell\mathbf{1}$ has approximately $p_\ell N$ zero elements. Taking advantage of this fact and the idea of compressed sensing, the SOAV optimization minimizes the weighted sum of absolute values $\|\boldsymbol{x} - r_\ell\mathbf{1}\|_1$ and $\|\boldsymbol{y} - \boldsymbol{A}\boldsymbol{x}\|_2^2$ as

$$\hat{\boldsymbol{b}} = \arg\min_{\boldsymbol{x}\in\mathbb{R}^N} \sum_{\ell=1}^L q_\ell \|\boldsymbol{x} - r_\ell\mathbf{1}\|_1 + \frac{\alpha}{2}\|\boldsymbol{y} - \boldsymbol{A}\boldsymbol{x}\|_2^2 \tag{2}$$

to obtain the estimate of $\boldsymbol{b}$, where α (> 0) is a parameter. The ℓ_1 norm in the objective function can also be considered as a convex relaxation of $\|\boldsymbol{x} - r_\ell\mathbf{1}\|_0$, which is large when $\boldsymbol{x}$ has many elements other than r_ℓ [11]. From the Bayesian perspective, the SOAV optimization uses the distribution $p_{\mathrm{pri}}(x) \propto \exp\left(-\sum_{\ell=1}^L q_\ell |x - r_\ell|\right)$ as the prior of the unknown variables. In the original SOAV optimization [17], the coefficients q_ℓ (≥ 0) are fixed as $q_\ell = p_\ell$, while the regularization-based method [11] solves (2) with $q_1 = \cdots = q_L = 1$. However, the validity of these selections has not been verified. We thus consider the coefficients as parameters to be optimized before solving (2), as described in Section III-B. Note that we can handle any discrete distribution by using the above formulation, while [19] and [20] considers only the case with symmetric distributions and the case with binary distributions, respectively.

B. DAMP

The derivation of DAMP begins with belief propagation with the sum-product algorithm [24] for a probability distribution corresponding to the SOAV optimization (2). We first consider the following joint probability distribution

$$\mu(\boldsymbol{x}) \propto \prod_{n=1}^{N} \exp\left(-\beta \sum_{\ell=1}^{L} q_\ell |x_n - r_\ell|\right) \cdot \prod_{m=1}^{M} \exp\left\{-\frac{\beta\alpha}{2}\left(y_m - \sum_{j=1}^{N} a_{m,j} x_j\right)^2\right\}, \quad (3)$$

where $\beta > 0$. Note that, as $\beta \to \infty$, the mass of the distribution concentrates on the solution of (2). Hence, we can solve (2) by calculating the mode of the marginal distribution of each x_n, which can be approximated via belief propagation. However, the computational complexity is prohibitive for the factor graph of (3) with large N.

To derive a low-complexity algorithm, we then consider the large system limit ($M, N \to \infty$ with fixed $M/N = \Delta$) and large β limit ($\beta \to \infty$), and approximate the sum-product algorithm for (3). As in the derivation in [22], assuming the measurement matrix $\boldsymbol{A} \in \mathbb{R}^{M\times N}$ being composed of i.i.d. variables with zero mean and variance $1/M$, we have the resultant algorithm as

$$\boldsymbol{z}^t = \boldsymbol{y} - \boldsymbol{A}\boldsymbol{x}^t + \frac{1}{\Delta}\boldsymbol{z}^{t-1}\left\langle \eta'\left(\boldsymbol{x}^{t-1} + \boldsymbol{A}^{\mathrm{T}}\boldsymbol{z}^{t-1}; \frac{\theta_{t-1}}{\sqrt{\Delta}}\right)\right\rangle, \quad (4)$$

$$\boldsymbol{x}^{t+1} = \eta\left(\boldsymbol{x}^t + \boldsymbol{A}^{\mathrm{T}}\boldsymbol{z}^t; \frac{\theta_t}{\sqrt{\Delta}}\right), \quad (5)$$

where $\boldsymbol{x}^t$ is the estimate of $\boldsymbol{b}$ at the tth iteration. The function $\eta(\cdot;\cdot)$ is given by

$$\eta(\boldsymbol{u}; c) = \mathrm{prox}_{cJ}(\boldsymbol{u}), \quad (6)$$

where $J(\boldsymbol{x}) = \sum_{\ell=1}^{L} q_\ell \|\boldsymbol{x} - r_\ell \boldsymbol{1}\|_1$ is the first term of the objective function in (2). By the direct calculation described in [4], the nth element of $\mathrm{prox}_{cJ}(\boldsymbol{u})$ is written as

$$[\mathrm{prox}_{cJ}(\boldsymbol{u})]_n = \begin{cases} u_n - cQ_1 & (u_n < r_1 + cQ_1) \\ r_1 & (r_1 + cQ_1 \le u_n < r_1 + cQ_2) \\ \vdots & \vdots \\ u_n - cQ_k & (r_{k-1} + cQ_k \le u_n < r_k + cQ_k) \\ r_k & (r_k + cQ_k \le u_n < r_k + cQ_{k+1}) \\ \vdots & \vdots \\ u_n - cQ_{L+1} & (r_L + cQ_{L+1} \le u_n) \end{cases}, \quad (7)$$

where u_n is the nth element of $\boldsymbol{u}$, $Q_1 = -\sum_{\ell=1}^{L} q_\ell$, $Q_{L+1} = \sum_{\ell=1}^{L} q_\ell$, and

$$Q_k = \sum_{\ell=1}^{k-1} q_\ell - \sum_{\ell'=k}^{L} q_{\ell'} \quad (k = 2, \ldots, L). \quad (8)$$

Since $[\mathrm{prox}_{cJ}(\boldsymbol{u})]_n$ is a function of only u_n, the function $\eta(\boldsymbol{u}; c)$ is a element-wise function of $\boldsymbol{u}$. The nth element of $\eta'(\boldsymbol{u}; c)$ in (4) is the partial derivative of $\eta(\boldsymbol{u}; c)$ with respect to u_n, and is given by $[\eta'(\boldsymbol{u}; c)]_n = 0$ if $[\mathrm{prox}_{cJ}(\boldsymbol{u})]_n \in \{r_1, \ldots, r_L\}$, otherwise $[\eta'(\boldsymbol{u}; c)]_n = 1$. $\theta_t^2 = \|\boldsymbol{x}^t - \boldsymbol{b}\|_2^2/N + \Delta\sigma_v^2$ is a scaled effective variance at the tth iteration [28]. Since the true solution $\boldsymbol{b}$ is unknown in practice, we use the alternative value for θ_t^2, e.g., $\hat{\theta}_t^2 = \|\boldsymbol{z}^t\|_2^2/N$ as in [29].

Algorithm 1 DAMP algorithm

Input: $\boldsymbol{y} \in \mathbb{R}^M$, $\boldsymbol{A} \in \mathbb{R}^{M\times N}$
Output: $\boldsymbol{x}^{T_{\mathrm{itr}}} \in \mathbb{R}^N$

1: $\boldsymbol{x}^0 = \boldsymbol{x}^1 = \mathrm{E}[\boldsymbol{b}]$, $\boldsymbol{z}^0 = \boldsymbol{0}$, $\Delta = M/N$
2: **for** $t = 1$ to $T_{\mathrm{itr}} - 1$ **do**
3: $\quad \boldsymbol{z}^t = \boldsymbol{y} - \boldsymbol{A}\boldsymbol{x}^t + \frac{1}{\Delta}\boldsymbol{z}^{t-1}\left\langle \eta'\left(\boldsymbol{x}^{t-1} + \boldsymbol{A}^{\mathrm{T}}\boldsymbol{z}^{t-1}; \frac{\hat{\theta}_{t-1}}{\sqrt{\Delta}}\right)\right\rangle$
4: $\quad \hat{\theta}_t^2 = \frac{\|\boldsymbol{z}^t\|_2^2}{N}$
5: $\quad \boldsymbol{x}^{t+1} = \eta\left(\boldsymbol{x}^t + \boldsymbol{A}^{\mathrm{T}}\boldsymbol{z}^t; \frac{\hat{\theta}_t}{\sqrt{\Delta}}\right)$
6: **end for**

We summarize the proposed DAMP algorithm in Algorithm 1. It should be noted that the update equations of DAMP (4), (5) are basically the same as those of the AMP algorithm for compressed sensing [21], [22]. The only difference is the function $\eta(\boldsymbol{u}; c)$, which is the soft thresholding function $[\eta(\boldsymbol{u}; c)]_n = \mathrm{sgn}(u_n)\max\{|u_n| - c, 0\}$ in the case of the sparse vector reconstruction. Hence, the function $\eta(\boldsymbol{u}; c)$ given by (6)–(8) can be considered as the soft thresholding function for the discrete-valued vector reconstruction. In TABLE I, we summarize the relationship between the original AMP algorithm and the proposed DAMP algorithm. From a Bayesian perspective, the original AMP algorithm uses the prior distribution $p_{\mathrm{pri}}(x) \propto \exp(-|x|)$ for the unknown sparse vector, whereas the DAMP algorithm uses $p_{\mathrm{pri}}(x) \propto \exp\left(-\sum_{\ell=1}^{L} q_\ell |x - r_\ell|\right)$ for the discrete-valued vector. Although the DAMP algorithm is based on the idea of the SOAV optimization, the estimate by the DAMP algorithm is not necessarily equal to that by the SOAV optimization because of the approximations in the derivation. For details of the relationship between AMP-based approaches and optimization-based approaches, see [30], [31]. Since (4) and (5) can be computed only with additions of vectors and multiplications of a matrix and a vector, the computational complexity of the algorithm is $O(MN)$ per iteration, which is lower than that of internal point methods $O(MN^2)$ used in [11].

The DAMP algorithm can also be used for complex-valued vector by rewriting the complex-valued model into the equivalent real model when the real and imaginary parts are independent, e.g., $\boldsymbol{b} \in \{1+j, -1+j, -1-j, 1-j\}^N$. When they are dependent, however, the algorithm cannot be directly applied and hence some extensions are required.

III. Asymptotic Analysis of DAMP

In this section, we provide a theoretical analysis of DAMP with state evolution framework [21], [25]. By using state

TABLE I
COMPARISON BETWEEN THE ORIGINAL AMP ALGORITHM AND THE PROPOSED DAMP ALGORITHM

	original AMP algorithm [21], [22]	proposed DAMP algorithm
purpose	sparse vector reconstruction (compressed sensing)	discrete-valued vector reconstruction
optimization problem	ℓ_1 optimization	SOAV optimization in (2)
prior distribution $p_{\text{pri}}(x)$	$p_{\text{pri}}(x) \propto \exp(-\lvert x\rvert)$	$p_{\text{pri}}(x) \propto \exp\left(-\sum_{\ell=1}^{L} q_\ell \lvert x - r_\ell\rvert\right)$
soft thresholding function	$[\eta(\boldsymbol{u};c)]_n = \text{sgn}(u_n)\max\{\lvert u_n\rvert - c, 0\}$	$\eta(\boldsymbol{u};c) = \text{prox}_{cJ}(\boldsymbol{u})$ in (7)

evolution, we give the required number of measurements for the perfect reconstruction and the parameter of the soft thresholding function minimizing the required number of measurements in the large system limit.

A. State Evolution

State evolution is a framework to analyze the asymptotic performance of the AMP algorithm. In the large system limit, the sample MSE $\sigma_t^2 = \|\boldsymbol{x}^t - \boldsymbol{b}\|_2^2/N$ of $\boldsymbol{x}^t$ can be predicted via the state evolution. Similarly to the case of compressed sensing, the state evolution formula for DAMP in Algorithm 1 is written as

$$\sigma_{t+1}^2 = \Psi\left(\sigma_t^2 + \Delta\sigma_v^2\right), \tag{9}$$

where

$$\Psi\left(\sigma^2\right) = \text{E}\left[\left\{\eta\left(X + \frac{\sigma}{\sqrt{\Delta}}Z; \frac{\sigma}{\sqrt{\Delta}}\right) - X\right\}^2\right]. \tag{10}$$

The random variable X has the same distribution as that of the unknown discrete variable, i.e., $\Pr(X = r_\ell) = p_\ell$ $(\ell = 1, \ldots, L)$ in our problem, and Z is the standard Gaussian random variable independent of X. In the rigorous proof for the state evolution [25], it is assumed that $\boldsymbol{A}$ is composed of i.i.d. Gaussian variables with zero mean and variance $1/M$, and $\eta(\cdot;\cdot)$ is Lipschitz continuous. In [25], however, it is expected that the state evolution is also valid for a broader class of measurement matrices $\boldsymbol{A}$, such as the matrices with i.i.d. (possibly non-Gaussian) elements with zero mean and variance $1/M$. In fact, some numerical results in [21] imply such universality of the state evolution.

B. Condition for Perfect Reconstruction by DAMP

We can analyze the performance of the DAMP algorithm by investigating the function $\Psi(\sigma^2)$, which can be analytically obtained (See Appendix A). In this section, we consider the noise-free case (i.e., $\sigma_v^2 = 0$) and investigate a sufficient condition for the perfect reconstruction defined as $\sigma_t^2 \to 0$ $(t \to \infty)$. Since we have $\Psi(0) = 0$ in the noise-free case, the sequence $\{\sigma_t^2\}_{t=0,1,\ldots}$ with the recursion (9) converges to zero if $\Psi(\sigma^2)$ is concave and its derivative at $\sigma^2 = 0$ is smaller than one, i.e., $\left.\frac{\text{d}\Psi}{\text{d}(\sigma^2)}\right|_{\sigma\downarrow 0} < 1$. In fact, the condition $\left.\frac{\text{d}\Psi}{\text{d}(\sigma^2)}\right|_{\sigma\downarrow 0} < 1$ results in $\Psi(\sigma^2) < \sigma^2$ and hence we have $\sigma_{t+1}^2 = \Psi(\sigma_t^2) < \sigma_t^2$. In this case, DAMP reconstructs the unknown vector $\boldsymbol{b}$ perfectly regardless of the initialization. Note that the above discussion is valid when the function $\Psi(\sigma^2)$ is concave, and we can examine the concavity as discussed later.

To obtain the condition for the perfect reconstruction, we evaluate $\left.\frac{\text{d}\Psi}{\text{d}(\sigma^2)}\right|_{\sigma\downarrow 0}$ analytically. By the mathematical manipulation, we have

$$\left.\frac{\text{d}\Psi}{\text{d}(\sigma^2)}\right|_{\sigma\downarrow 0} := D(\boldsymbol{Q}) \tag{11}$$

$$= \frac{1}{\Delta}\sum_{\ell=1}^{L} p_\ell \left\{Q_\ell\phi\left(Q_\ell\right) - Q_{\ell+1}\phi\left(Q_{\ell+1}\right) + \left(1 + Q_\ell^2\right)\Phi\left(Q_\ell\right) + \left(1 + Q_{\ell+1}^2\right)\left(1 - \Phi\left(Q_{\ell+1}\right)\right)\right\}, \tag{12}$$

where $\boldsymbol{Q} = [Q_1 \ \cdots \ Q_{L+1}]^{\text{T}}$ (See Appendix B). Since we can choose any $q_1, \ldots, q_L \geq 0$ in (2), we minimize (12) with respect to $Q_1, \ldots, Q_{L+1}$ as

$$D_{\min} = \min_{\boldsymbol{Q}} D(\boldsymbol{Q}) \text{ subject to } Q_1 \leq \cdots \leq Q_{L+1}. \tag{13}$$

Note that, in (13), we eliminate the constraint $Q_1 = -Q_{L+1}$. As we will see later, the optimal values of Q_1 and Q_{L+1} are $Q_1^{\text{opt}} = -\infty$ and $Q_{L+1}^{\text{opt}} = \infty$, respectively, and hence this relaxation does not change the optimal value $D_{\min}$. The optimization problem (13) can be solved via interior point methods [14] because $D(\boldsymbol{Q})$ is a convex function of $\boldsymbol{Q}$. We can also solve (13) with the following theorem, which enables us to theoretically analyze the performance of DAMP in some cases as described in Section III-C. In what follows, for an equation $h(Q) = 0$ with a unique solution, we denote the solution by $\hat{Q}(h(Q))$, i.e., $h(\hat{Q}(h(Q))) = 0$.

Theorem 1. The unique minimizer $\boldsymbol{Q}^{\text{opt}} = \left[Q_1^{\text{opt}} \ \cdots \ Q_{L+1}^{\text{opt}}\right]^{\text{T}}$ of the optimization problem (13) can be obtained by Algorithm 2.

Proof: See Appendix C. ∎

By using Algorithm 2, we can obtain the unique minimizer $\boldsymbol{Q}^{\text{opt}}$ and the corresponding minimum value $D_{\min}$ of $\left.\frac{\text{d}\Psi}{\text{d}(\sigma^2)}\right|_{\sigma\downarrow 0}$. From (7), the soft thresholding function with the optimal parameters Q_ℓ^{opt} is written as

$$\left[\eta^{\text{S}}\left(\boldsymbol{u};c\right)\right]_n = \begin{cases} r_1 & \left(u_n < r_1 + cQ_2^{\text{opt}}\right) \\ \vdots & \vdots \\ u_n - cQ_k^{\text{opt}} & \left(r_{k-1} + cQ_k^{\text{opt}} \leq u_n < r_k + cQ_k^{\text{opt}}\right) \\ r_k & \left(r_k + cQ_k^{\text{opt}} \leq u_n < r_k + cQ_{k+1}^{\text{opt}}\right) \\ \vdots & \vdots \\ r_L & \left(r_L + cQ_L^{\text{opt}} \leq u_n\right) \end{cases}, \tag{14}$$

Algorithm 2 Parameter optimization

Input: $p_1, \ldots, p_L$
Output: $\boldsymbol{Q}^{\text{opt}} = \left[Q_1^{\text{opt}} \ \cdots \ Q_{L+1}^{\text{opt}}\right]^{\text{T}}$

for $\ell = L, L-1, \ldots, 2$ **do**
  $F_\ell(Q) = p_{\ell-1}\left\{-\phi\left(Q\right) + Q\left(1-\Phi\left(Q\right)\right)\right\}$
  $\quad + p_\ell\left\{\phi\left(Q\right) + Q\Phi\left(Q\right)\right\}$
end for
$Q_{L+1}^{\text{opt}} = \infty$
$G_L(Q) = F_L(Q)$
for $\ell = L, L-1, \ldots, 3$ **do**
  if $\hat{Q}(G_\ell(Q)) > \max\limits_{j=2,\ldots,\ell-1} \hat{Q}\left(\sum_{k=j}^{\ell-1} F_k(Q)\right)$ **then**
    $Q_\ell^{\text{opt}} = \hat{Q}(G_\ell(Q))$
    $G_{\ell-1}(Q) = F_{\ell-1}(Q)$
  else
    $Q_\ell^{\text{opt}} = Q_{\ell-1}^{\text{opt}}$
    $G_{\ell-1}(Q) = F_{\ell-1}(Q) + G_\ell(Q)$
  end if
end for
$Q_2^{\text{opt}} = \hat{Q}(G_2(Q))$
$Q_1^{\text{opt}} = -\infty$

where $\left[\eta^{\text{S}}\left(\boldsymbol{u}; c\right)\right]_n$ denotes the nth element of $\eta^{\text{S}}(\boldsymbol{u}; c)$.

The DAMP algorithm with $\eta^{\text{S}}(\cdot;\cdot)$, which we call *soft thresholding DAMP* henceforth, provides the perfect reconstruction in the large system limit if $D_{\min} < 1$ and the function $\Psi^{\text{S}}(\sigma^2) = \text{E}\left[\left\{\eta^{\text{S}}\left(X + \frac{\sigma}{\sqrt{\Delta}}Z; \frac{\sigma}{\sqrt{\Delta}}\right) - X\right\}^2\right]$ is concave. Since we have

$$\frac{\text{d}^2\Psi}{\text{d}(\sigma^2)^2} = \frac{\sqrt{\Delta}}{2\sigma^5}\sum_{\ell=1}^{L} p_\ell \sum_{k=1}^{L}\left(-r_\ell + r_k\right)^3\left\{-\phi\left(T_{\ell,k,k}\right) + \phi\left(T_{\ell,k,k+1}\right)\right\}, \tag{15}$$

where $T_{\ell,k,k'} = \frac{\sqrt{\Delta}}{\sigma}\left(-r_\ell + r_k\right) + Q_{k'}$ (See Appendix D), the concavity of $\Psi(\sigma^2)$ depends on Q_ℓ. By evaluating (15) with $\boldsymbol{Q} = \boldsymbol{Q}^{\text{opt}}$, we can investigate whether $\Psi^{\text{S}}(\sigma^2)$ is concave or not. If $\Psi^{\text{S}}(\sigma^2)$ is concave and $D_{\min} < 1$, soft thresholding DAMP can perfectly reconstruct the discrete-valued vector in the large system limit.

C. Examples of Asymptotic Analysis

We show three examples of the analysis for DAMP via state evolution. In all examples, we can confirm that $\Psi^{\text{S}}(\sigma^2)$ is concave by the direct calculation.

Example 1 (Binary vector). As the simplest example, we firstly consider the reconstruction of a binary vector $\boldsymbol{b} \in \{r_1, r_2\}^N$ with $\Pr(b_n = r_1) = p_1$ and $\Pr(b_n = r_2) = p_2\ (= 1 - p_1)$. The binary vector reconstruction appears in CDMA multiuser detection and signal detection for MIMO systems with binary phase shift keying (BPSK) or quadrature phase shift keying (QPSK). By using Algorithm 2, we can obtain the optimal parameters of the soft thresholding function.

In the noise-free case, soft thresholding DAMP provides the perfect reconstruction in the large system limit if $D_{\min} < 1$.

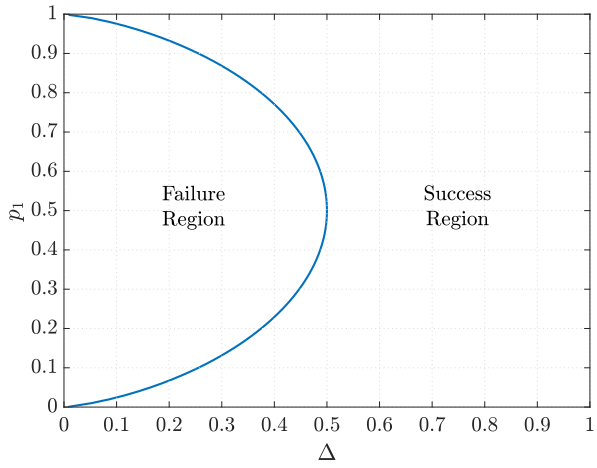

Fig. 1. Phase transition of soft thresholding DAMP for binary vector

Figure 1 shows the phase transition line of soft thresholding DAMP, where $D_{\min} = 1$. Note that the line is the boundary between the success and failure regions of DAMP in the large system limit. In the left region of the curve, the MSE of the estimate obtained by DAMP does not converge to zero. In the right region, DAMP can provide the perfect reconstruction of $\boldsymbol{b}$. For example, the figure shows that DAMP requires at least $N/2$ observations to accurately reconstruct an N-dimensional uniformly distributed binary vector with $p_1 = 0.5$. This result coincides with the theoretical analysis for the regularization-based method and the transform-based method [11] as well as the box relaxation [16]. Moreover, our analysis also provides the required number of measurements for the asymmetric distribution with $p_1 \neq 0.5$, which has not been obtained in [11] and [16]. It should be noted that $D_{\min}$ in (13) is independent of r_1 and r_2, and hence the phase transition line in Fig. 1 is identical for any r_1 and r_2 in the noise-free case.

In the noisy case, the asymptotic MSE at the fixed point of soft thresholding DAMP, i.e., the value of σ^2 satisfying $\sigma^2 = \Psi^{\text{S}}(\sigma^2 + \Delta\sigma_v^2)$, can be obtained numerically by iterating $\sigma_{t+1}^2 = \Psi^{\text{S}}(\sigma_t^2 + \Delta\sigma_v^2)$. Figure 2 shows the result for the binary vector $\boldsymbol{b} \in \{-1, 1\}^N$ with $\Pr(b_n = -1) = p_1$, $\Pr(b_n = 1) = 1 - p_1$, and $\sigma_v^2 = 0.01$. We can see that the asymptotic MSE becomes smaller when the measurement ratio Δ increases.

Example 2 (Possibly sparse discrete-valued vector). The reconstruction of a possibly sparse discrete-valued vector, such as $\boldsymbol{b} \in \{-1, 0, 1\}^N$ and $\boldsymbol{b} \in \{-3, -1, 0, 1, 3\}^N$, also arises in some problems, e.g., multiuser detection for machine-to-machine communications [4] and error recovery for MIMO signal detection [32]. Although some methods have been proposed for the reconstruction of the discrete-valued sparse vector [33]–[37], their theoretical analyses have not been obtained.

In Fig. 3, we show the phase transition line for $\boldsymbol{b} \in \{-r, 0, r\}^N$ and $\boldsymbol{b} \in \{-3r, -r, 0, r, 3r\}^N$ $(r > 0)$ in the noise-free case. For $\boldsymbol{b} \in \{-r, 0, r\}^N$, we assume $\Pr(b_n = 0) = p$ and $\Pr(b_n = -r) = \Pr(b_n = r) = (1-p)/2$. For $\boldsymbol{b} \in \{-3r, -r, 0, r, 3r\}^N$, we assume $\Pr(b_n = 0) = p$ and $\Pr(b_n = -3r) = \Pr(b_n = -r) = \Pr(b_n = r) = \Pr(b_n = 3r) = (1-p)/4$. The dashed line shows the phase transition

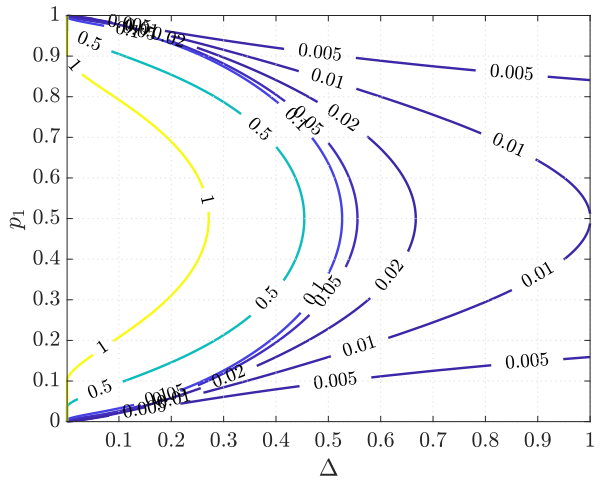

Fig. 2. MSE at the fixed point in the noisy case ($\boldsymbol{b} \in \{-1, 1\}^N$, $\Pr(b_n = -1) = p_1$, $\Pr(b_n = 1) = 1 - p_1$, $\sigma_v^2 = 0.01$)

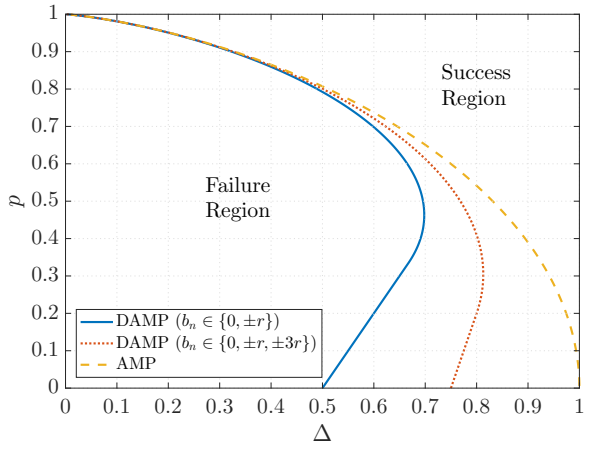

Fig. 3. Phase transition of soft thresholding DAMP for possibly sparse discrete-valued vector

line of the original AMP algorithm for compressed sensing, which utilizes only the sparsity of the unknown vector. If the unknown vector is discrete-valued, the DAMP algorithm requires a less number of measurements compared to the AMP algorithm. However, as the possible candidates for non-zero value increases, more number of measurements is required for the perfect reconstruction.

Example 3 (Uniformly distributed discrete-valued vector). Finally, we analyze the reconstruction of $\boldsymbol{b} \in \{r_1, \ldots, r_L\}^N$ with the uniform distribution $p_1 = \cdots = p_L = 1/L$. The signal detection for MIMO systems with quadrature amplitude modulation (QAM) can be reduced to such reconstruction problem.

By Algorithm 2, we have $Q_L^{\text{opt}} = \cdots = Q_2^{\text{opt}} = 0$. The resultant soft thresholding function is equivalent to that of the AMP algorithm with the box relaxation [38]. The condition for the perfect reconstruction in the noise-free case is $D_{\min} = (L-1)/(\Delta L) < 1 \Leftrightarrow \Delta > (L-1)/L$, which means that soft thresholding DAMP requires more than $(L-1)N/L$ measurements to reconstruct a N dimensional vector with the uniform distribution of L values. This threshold is the same as that for the transform-based method [11]. It should be noted that the analysis of DAMP can also be applied even for non-uniform distribution, while uniform distributions are assumed for the analyses in [11] and [38].

IV. Application to SOAV Optimization

In this section, we propose a method to determine the parameters q_ℓ of the SOAV optimization (2) on the basis of the asymptotic analysis of soft thresholding DAMP.

The DAMP algorithm proposed in the previous section has low computational complexity and its asymptotic performance can be predicted by state evolution, which provides the optimal parameters of the soft thresholding function. In the derivation, however, we take the large system limit and assume that the measurement matrix $\boldsymbol{A}$ is composed of i.i.d. elements. Hence, the DAMP algorithm suffers from the performance degradation when the problem size is not large or the measurement matrix is composed of correlated elements.

The SOAV optimization can be solved with the proximal splitting methods [18] as a convex optimization problem [4], [7]. The convex optimization algorithms do not require any assumptions on the measurement matrix and can obtain the minimizer even when the problem size is small. Thus, when the measurement matrix is composed of correlated elements or the problem size is not large enough, the convex optimization-based approach using parameters $q_1, \ldots, q_L$ obtained from the optimal values $Q_1^{\text{opt}}, \ldots, Q_L^{\text{opt}}$ in the previous section might outperform the DAMP algorithm.

We thus derive the parameters q_ℓ^{opt} corresponding to the optimal parameters Q_ℓ^{opt} in a casual manner. From the definitions of Q_k in (8), we can obtain q_ℓ from Q_ℓ and $Q_{\ell+1}$ as $q_\ell = (-Q_\ell + Q_{\ell+1})/2$. Since $Q_2^{\text{opt}}, \ldots, Q_L^{\text{opt}}$ are finite, the corresponding coefficients $q_2^{\text{opt}}, \ldots, q_{L-1}^{\text{opt}}$ given by

$$q_\ell^{\text{opt}} = \frac{1}{2}\left(-Q_\ell^{\text{opt}} + Q_{\ell+1}^{\text{opt}}\right) \tag{16}$$

are also finite. On the other hand, $q_1^{\text{opt}} = q_L^{\text{opt}} = \infty$ follows from $Q_1^{\text{opt}} = -\infty$ and $Q_{L+1}^{\text{opt}} = \infty$. The objective function of the SOAV optimization includes q_1^{opt} and q_L^{opt} in the form $q_1^{\text{opt}}|x - r_1| + q_L^{\text{opt}}|x - r_L|$, and the term becomes infinity when $x \le r_1$ or $x \ge r_L$. When $r_1 < x < r_L$, however, the term is computed as

$$q_1^{\text{opt}}|x - r_1| + q_L^{\text{opt}}|x - r_L| = (q_1^{\text{opt}} - q_L^{\text{opt}})x + \text{const.} \tag{17}$$

$$= \frac{1}{2}(Q_2^{\text{opt}} + Q_L^{\text{opt}}) + \text{const.} \tag{18}$$

because we have

$$Q_2 + Q_L = 2(q_1 - q_L) \tag{19}$$

from (8), where "const." is a constant independent of x. Since Q_2^{opt} and Q_L^{opt} are finite, $Q_2^{\text{opt}} + Q_L^{\text{opt}}$ is also finite and hence we have

$$q_1^{\text{opt}}|x - r_1| + q_L^{\text{opt}}|x - r_L| = \begin{cases} \frac{1}{2}(Q_2^{\text{opt}} + Q_L^{\text{opt}})x + \text{const.} & (r_1 < x < r_L) \\ \infty & (\text{otherwise}) \end{cases}, \tag{20}$$

Algorithm 3 Beck-Teboulle proximal gradient algorithm for SOAV optimization (21)

Input: $\boldsymbol{y} \in \mathbb{R}^M, \boldsymbol{A} \in \mathbb{R}^{M \times N}, \alpha \in \mathbb{R}$
Output: $\boldsymbol{x}^{T_{\rm itr}} \in \mathbb{R}^N$
1: $\boldsymbol{x}^1 = \boldsymbol{0}$, $\boldsymbol{z}^1 = \boldsymbol{0}$, $\tau_1 = 1$, $\gamma \geq \alpha \|\boldsymbol{A}\|_2^2$
2: **for** $t = 1$ to $T_{\rm itr} - 1$ **do**
3: $\quad \boldsymbol{x}^{t+1} = \eta^{\rm S}\left(\boldsymbol{z}^t + \gamma^{-1}\alpha \boldsymbol{A}^{\rm T}\left(\boldsymbol{y} - \boldsymbol{A}\boldsymbol{z}^t\right); \gamma^{-1}\right)$
4: $\quad \tau_{t+1} = \dfrac{1 + \sqrt{4\tau_t^2 + 1}}{2}$
5: $\quad \lambda_t = 1 + \dfrac{\tau_t - 1}{\tau_{t+1}}$
6: $\quad \boldsymbol{z}^{t+1} = \lambda_t \boldsymbol{x}^{t+1} + (1 - \lambda_t)\, \boldsymbol{x}^t$
7: **end for**

where the infinity for $x \notin (r_1, r_L)$ corresponds to the box constraint $r_1 < x < r_L$. Therefore, we have the SOAV optimization problem corresponding to the optimal parameters for soft thresholding DAMP as

$$\hat{\boldsymbol{b}} = \arg\min_{\boldsymbol{x} \in \mathbb{R}^N} \sum_{\ell=1}^{L} q_\ell^{\rm opt} \|\boldsymbol{x} - r_\ell \boldsymbol{1}\|_1 + \frac{\alpha}{2}\|\boldsymbol{y} - \boldsymbol{A}\boldsymbol{x}\|_2^2 \quad \text{subject to} \quad r_1 \boldsymbol{1} \leq \boldsymbol{x} \leq r_L \boldsymbol{1}, \tag{21}$$

where $q_2^{\rm opt}, \ldots, q_{L-1}^{\rm opt}$ are given by (16) and $q_1^{\rm opt}$, $q_L^{\rm opt}$ (≥ 0) must be chosen to satisfy $q_1^{\rm opt} - q_L^{\rm opt} = (Q_2^{\rm opt} + Q_L^{\rm opt})/2$. Note that we relax the constraint as $r_1 \boldsymbol{1} \leq \boldsymbol{x} \leq r_L \boldsymbol{1}$ because the unknown vector $\boldsymbol{b}$ may have r_1 and r_L. The problem (21) can be rewritten as

$$\hat{\boldsymbol{b}} = \arg\min_{\boldsymbol{x} \in \mathbb{R}^N} h_1(\boldsymbol{x}) + h_2(\boldsymbol{x}), \tag{22}$$

where $h_1(\boldsymbol{x}) = \sum_{\ell=1}^{L} q_\ell^{\rm opt} \|\boldsymbol{x} - r_\ell \boldsymbol{1}\|_1 + \iota(\boldsymbol{x})$, $h_2(\boldsymbol{x}) = \alpha \|\boldsymbol{y} - \boldsymbol{A}\boldsymbol{x}\|_2^2/2$, and

$$\iota(\boldsymbol{x}) = \begin{cases} 0 & (r_1 \boldsymbol{1} \leq \boldsymbol{x} \leq r_L \boldsymbol{1}) \\ \infty & (\text{otherwise}) \end{cases}. \tag{23}$$

An important fact here is that the proximity operator of $h_1(\boldsymbol{x})$ is given by $\mathrm{prox}_{ch_1}(\boldsymbol{u}) = \eta^{\rm S}(\boldsymbol{u}; c)$ because $q_1^{\rm opt}, \ldots, q_L^{\rm opt}, Q_1^{\rm opt}, \ldots, Q_L^{\rm opt}$ satisfy (8) and $\iota(\cdot)$ restricts the value of $\mathrm{prox}_{ch_1}(\boldsymbol{u})$ as $r_1 \leq [\mathrm{prox}_{ch_1}(\boldsymbol{u})]_n \leq r_L$. Hence, the convex optimization problem (21) can be efficiently solved by proximal splitting methods [18] using $\eta^{\rm S}(\boldsymbol{u}; c)$. As an example, we show Beck-Teboulle proximal gradient algorithm [18], [39] for the optimization problem (22) in Algorithm 3.

As we can see from the following example, the proposed parameters $q_\ell^{\rm opt}$ are different from those of the original SOAV optimization in general.

Example 4. We consider the reconstruction of $\boldsymbol{b} \in \{-1, 0, 1\}^N$. The distribution of $\boldsymbol{b}$ is assumed to be $\Pr(b_n = 0) = 0.2$ and $\Pr(b_n = -1) = \Pr(b_n = 1) = 0.4$. In this case, we have $Q_1^{\rm opt} = -\infty$, $Q_2^{\rm opt} = Q_3^{\rm opt} = 0$, and $Q_4^{\rm opt} = \infty$ by Algorithm 2. Hence, the proposed parameters satisfy $q_1^{\rm opt} - q_3^{\rm opt} = 0$ and $q_2^{\rm opt} = 0$. Since we have $q_1^{\rm opt}\|\boldsymbol{x}+\boldsymbol{1}\|_1 + q_2^{\rm opt}\|\boldsymbol{x}\|_1 + q_3^{\rm opt}\|\boldsymbol{x}-\boldsymbol{1}\|_1 = 2q_1^{\rm opt} N$ (= const.) for $-\boldsymbol{1} \leq \boldsymbol{x} \leq \boldsymbol{1}$ in this case, the proposed optimization problem is given by

$$\hat{\boldsymbol{b}} = \arg\min_{\boldsymbol{x} \in \mathbb{R}^N} \|\boldsymbol{y} - \boldsymbol{A}\boldsymbol{x}\|_2^2 \quad \text{subject to} \quad -\boldsymbol{1} \leq \boldsymbol{x} \leq \boldsymbol{1}. \tag{24}$$

The optimization problem (24) is quite different from the original SOAV optimization [17] and the regularization-based method [11], where $(q_1, q_2, q_3) = (0.4, 0.2, 0.4)$ and $(q_1, q_2, q_3) = (1, 1, 1)$, respectively. Note that the box relaxation optimization (24) has been considered for the reconstruction of the binary vector $\boldsymbol{b} \in \{-1, 1\}^N$ (e.g., [15], [16]). The proposed approach results in the box relaxation optimization (24) even when $\Pr(b_j = 0) = 0.2$.

V. Bayes optimal DAMP

In this section, we provide Bayes optimal DAMP based on the state evolution. In the DAMP algorithm in Algorithm 1, we can use different functions as $\eta(\cdot;\cdot)$ instead of the soft thresholding function (7), (14). Moreover, the state evolution formula (9) is still valid for different $\eta(\cdot;\cdot)$ as far as it is Lipschitz continuous. In the literature of compressed sensing, the AMP algorithm is called *Bayes optimal* if the function $\left[\eta^{\rm B}(\boldsymbol{u}; c)\right]_n = \mathrm{E}\left[X \,|\, X + cZ = u_n\right]$ is used instead of the soft thresholding function [29], [40]. Note that $\eta^{\rm B}\left(\cdot; \dfrac{\sigma}{\sqrt{\Delta}}\right)$ is the minimizer of $\tilde{\Psi}(\sigma^2) = \mathrm{E}\left[\left\{\tilde{\eta}\left(X + \dfrac{\sigma}{\sqrt{\Delta}} Z\right) - X\right\}^2\right]$ when we consider $\tilde{\Psi}(\sigma^2)$ as the functional of a function $\tilde{\eta}(\cdot)$.

Although it is difficult in general to analytically calculate the optimal function $\eta^{\rm B}(\cdot;\cdot)$, we can obtain $\eta^{\rm B}(\cdot;\cdot)$ for the Bayes optimal DAMP because the distribution of X is discrete in our problem. The conditional probability of X can be written as

$$\Pr\left(X = r_\ell \,|\, X + cZ = u_n\right) = \frac{1}{\zeta} p_\ell \phi\left(\frac{u_n - r_\ell}{c}\right), \tag{25}$$

where the normalizing constant ζ is given by $\zeta = \sum_{\ell=1}^{L} p_\ell \phi\left(\dfrac{u_n - r_\ell}{c}\right)$. From (25), we have

$$\left[\eta^{\rm B}(\boldsymbol{u}; c)\right]_n = \frac{\sum_{\ell=1}^{L} p_\ell r_\ell \phi\left(\dfrac{u_n - r_\ell}{c}\right)}{\sum_{\ell'=1}^{L} p_{\ell'} \phi\left(\dfrac{u_n - r_{\ell'}}{c}\right)}. \tag{26}$$

As a special case, when $r_1 = -1, r_2 = 1$ and $p_1 = p_2 = 0.5$, (26) can be reduced to $\left[\eta^{\rm B}(\boldsymbol{u}; c)\right]_n = \tanh\left(u_n/c^2\right)$, which has been proposed for CDMA multiuser detection [2], [41].

The state evolution formula for Bayes optimal DAMP is given by $\sigma_{t+1}^2 = \Psi^{\rm B}(\sigma_t^2 + \Delta\sigma_v^2)$, where $\Psi^{\rm B}(\sigma^2) = \mathrm{E}\left[\left\{\eta^{\rm B}\left(X + \dfrac{\sigma}{\sqrt{\Delta}} Z; \dfrac{\sigma}{\sqrt{\Delta}}\right) - X\right\}^2\right]$. Since $\eta^{\rm B}\left(\cdot; \dfrac{\sigma}{\sqrt{\Delta}}\right)$ is the minimizer of $\tilde{\Psi}(\sigma^2)$, Bayes optimal DAMP provides the minimum MSE at each iteration in the large system limit. In the noise-free case, the sequence of the MSE $\{\sigma_t^2\}_{t=0,1,\ldots}$

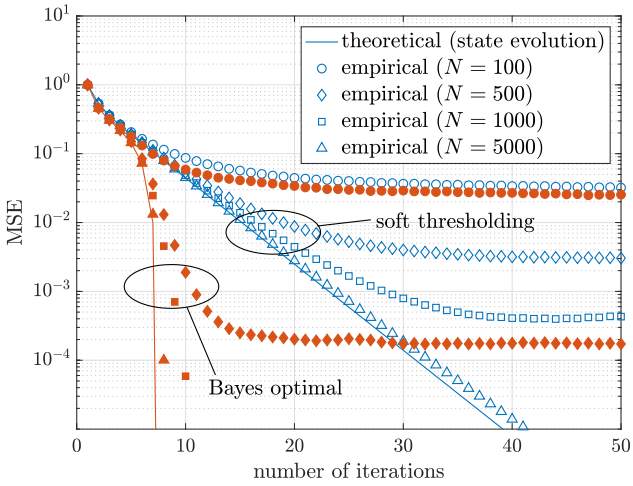

Fig. 4. State evolution and empirical performance in the noise-free case ($\boldsymbol{b} \in \{-1, 1\}^N$, $\Pr(b_j = -1) = 0.2$, $\Pr(b_j = 1) = 0.8$, $\Delta = 0.5$, and $\sigma_v^2 = 0$)

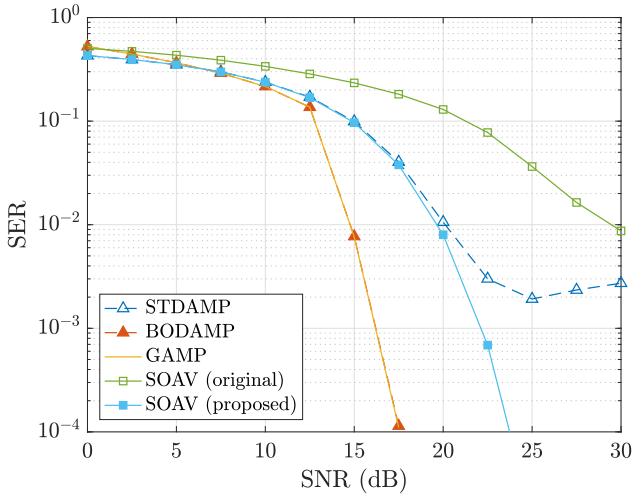

Fig. 5. SER for i.i.d. Gaussian matrix ($\boldsymbol{b} \in \{-1, 0, 1\}^N$, $\Pr(b_n = 0) = 0.2$, $\Pr(b_n = -1) = \Pr(b_n = 1) = 0.4$, and $(N, M) = (1000, 800)$)

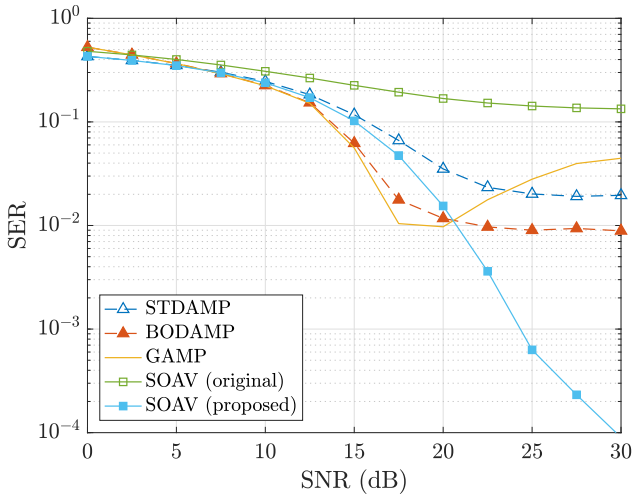

Fig. 6. SER for i.i.d. Gaussian matrix ($\boldsymbol{b} \in \{-1, 0, 1\}^N$, $\Pr(b_n = 0) = 0.2$, $\Pr(b_n = -1) = \Pr(b_n = 1) = 0.4$, and $(N, M) = (100, 80)$)

obtained by $\sigma_{t+1}^2 = \Psi^{\mathrm{B}}(\sigma_t^2)$ converges to zero if $\Psi^{\mathrm{S}}(\sigma^2)$ is concave and $D_{\min} < 1$, because $\Psi^{\mathrm{S}}(\sigma^2) < \sigma^2$ in that case and hence $\sigma_{t+1}^2 = \Psi^{\mathrm{B}}(\sigma_t^2) \leq \Psi^{\mathrm{S}}(\sigma_t^2) < \sigma_t^2$. Thus, the required measurement ratio Δ for soft thresholding DAMP is an upper bound of that for Bayes optimal DAMP. However, since $\Psi^{\mathrm{B}}(\sigma^2)$ is not necessarily concave unlike $\Psi^{\mathrm{S}}(\sigma^2)$, it is difficult to obtain the necessary condition analytically for the perfect reconstruction by Bayes optimal DAMP.

A similar algorithm to Bayes optimal DAMP can be derived by using the discrete prior distribution in generalized AMP (GAMP) [42], [43] with scalar variances. The AMP-based algorithm similar to Bayes optimal DAMP has also been proposed for MIMO signal detection [44], where the reconstruction of complex discrete-valued vectors with uniform distributions is considered. However, these algorithms use update equations to obtain the effective variance, while the proposed DAMP algorithm uses the simple estimation $\hat{\theta}_t^2 = \|\boldsymbol{z}^t\|_2^2/N$. These conventional algorithms use the knowledge of the noise variance σ_v^2 unlike Bayes optimal DAMP.

VI. Simulation Results

In this section, we evaluate the performance of the proposed algorithms via computer simulations.

Figure 4 shows the prediction of MSE via state evolution and the empirical MSE $\sigma_t^2 = \|\boldsymbol{x}^t - \boldsymbol{b}\|_2^2/N$ with DAMP obtained by simulations. We set $\boldsymbol{b} \in \{-1, 1\}^N$, $\Pr(b_j = -1) = 0.2$, $\Pr(b_j = 1) = 0.8$, $\Delta = 0.5$, and $\sigma_v^2 = 0$. We evaluate the performance for the different problem sizes of $N = 100, 500, 1000$, and 5000. The measurement matrix $\boldsymbol{A} \in \mathbb{R}^{M \times N}$ is composed of i.i.d. Gaussian variables with zero mean and variance $1/M$. In the figure, "soft thresholding" denotes the performance of DAMP with the soft thresholding function $\eta^{\mathrm{S}}(\cdot; \cdot)$ and "Bayes optimal" denotes that of Bayes optimal DAMP with $\eta^{\mathrm{B}}(\cdot; \cdot)$. We can see that Bayes optimal DAMP has much smaller MSE with less number of iterations than soft thresholding DAMP. The figure also shows that the prediction with state evolution is close to the empirical performance in the large-scale systems.

In Figs. 5 and 6, we evaluate the average of SER defined as $\|\mathcal{Q}(\boldsymbol{x}^t) - \boldsymbol{b}\|_0/N$, where $\mathcal{Q}(\boldsymbol{x}) = \arg\min_{\tilde{\boldsymbol{b}} \in \{r_1, \ldots, r_L\}^N} \|\tilde{\boldsymbol{b}} - \boldsymbol{x}\|_1$. The distribution of the unknown vector is $\Pr(b_n = 0) = 0.2, \Pr(b_n = -1) = \Pr(b_n = 1) = 0.4$, which has been considered in Example 4. The problem size is $(N, M) = (1000, 800)$ in Fig. 5 and $(N, M) = (100, 80)$ in Fig. 6. The measurement matrix $\boldsymbol{A} \in \mathbb{R}^{M \times N}$ is composed of i.i.d. Gaussian variables with zero mean and variance $1/M$, and the SNR is defined as $N(1-p)/\left(M\sigma_v^2\right)$. The number of iterations in the algorithms is fixed to 200. In the figures, "STDAMP" and "BODAMP" denote soft thresholding DAMP and Bayes optimal DAMP, respectively. For comparison, we also plot the performance of sum-product GAMP [42] with the discrete-prior distribution as "GAMP". "SOAV (original)" and "SOAV (proposed)" represent the SOAV optimization with the original coefficients $q_\ell = p_\ell$ [17] and that with the proposed parameters q_ℓ^{opt}, respectively. The parameter for the original SOAV optimization α is fixed as $\alpha = 10$. In the simulation, we have used Beck-Teboulle proximal gradient algorithm [18], [39] to solve these optimization problems. In both figures, we

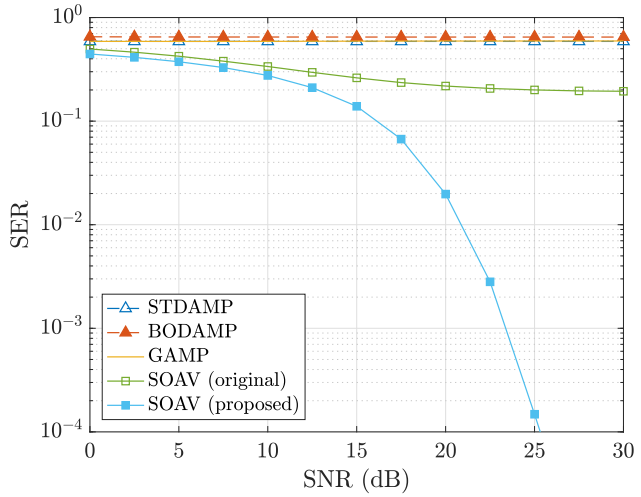

Fig. 7. SER for correlated matrix ($\boldsymbol{b} \in \{-1, 0, 1\}^N$, $\Pr(b_n = 0) = 0.2$, $\Pr(b_n = -1) = \Pr(b_n = 1) = 0.4$, and $(N, M) = (1000, 800)$)

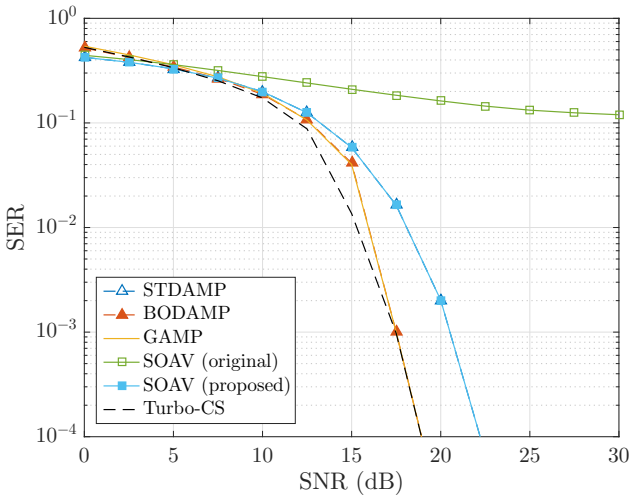

Fig. 8. SER for partial DCT matrix ($\boldsymbol{b} \in \{-1, 0, 1\}^N$, $\Pr(b_n = 0) = 0.2$, $\Pr(b_n = -1) = \Pr(b_n = 1) = 0.4$, and $(N, M) = (1024, 768)$)

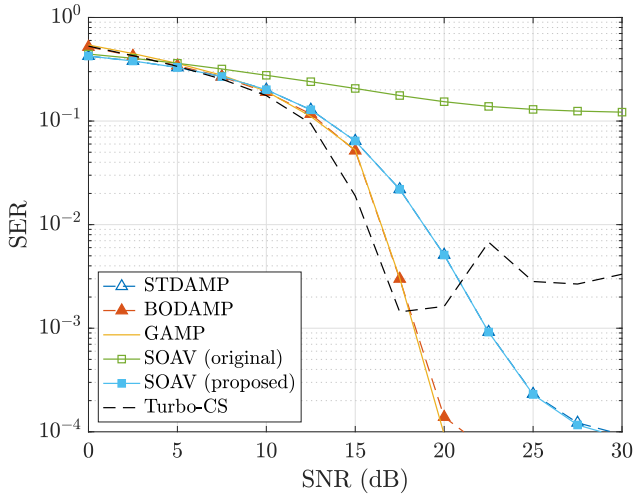

Fig. 9. SER for partial DCT matrix ($\boldsymbol{b} \in \{-1, 0, 1\}^N$, $\Pr(b_n = 0) = 0.2$, $\Pr(b_n = -1) = \Pr(b_n = 1) = 0.4$, and $(N, M) = (128, 96)$)

can see that the performance of the SOAV optimization with the proposed parameters is much better than the original ones. In Fig. 5, where $N = 1000$, Bayes optimal DAMP and GAMP have better SER performance than the other methods. As mentioned in Section V, the GAMP algorithm uses the knowledge of the noise variance, which is not necessary in the proposed Bayes optimal DAMP. For the smaller-scale problem in Fig. 6, however, the performance of these methods severely degrades and the SOAV optimization with the proposed parameters can achieve the best SER performance for high SNR region. The difference of the error floor between Bayes optimal DAMP and GAMP may be caused by the estimation of the effective variance described in Section V.

In Fig. 7, we show the SER performance for the correlated measurement matrix $\boldsymbol{A} = \boldsymbol{\Phi}_{\mathrm{R}}^{\frac{1}{2}} \boldsymbol{A}_{\text{i.i.d.}} \boldsymbol{\Phi}_{\mathrm{T}}^{\frac{1}{2}}$. Here, $\boldsymbol{A}_{\text{i.i.d.}} \in \mathbb{R}^{M \times N}$ is composed of i.i.d. Gaussian variables with zero mean and variance $1/M$. The (i, j) elements of the positive definite matrices $\boldsymbol{\Phi}_{\mathrm{R}}$ and $\boldsymbol{\Phi}_{\mathrm{T}}$ are given by $[\boldsymbol{\Phi}_{\mathrm{R}}]_{i,j} = J_0(|i-j| \cdot 2\pi d_{\mathrm{R}}/\nu)$ and $[\boldsymbol{\Phi}_{\mathrm{T}}]_{i,j} = J_0(|i-j| \cdot 2\pi d_{\mathrm{T}}/\nu)$, respectively. $J_0(\cdot)$ is the zeroth-order Bessel function of the first kind and we set $d_{\mathrm{R}} = d_{\mathrm{T}} = \nu/2$ in the simulation. This model has been used for spatially correlated MIMO channels with equally spaced antennas [45]. The problem size and the distribution of the unknown vector are the same as those in Fig. 5. From Fig. 7, we can see that the performance of AMP-based algorithms severely degrades because of the correlation. On the other hand, the approach based on the SOAV optimization with the proposed parameters works well even for the correlated measurement matrix.

Next, we evaluate the SER performance when the measurement matrix is a partial DCT matrix. The measurement vector $\boldsymbol{y}$ is assumed to be written as

$$\boldsymbol{y} = \boldsymbol{S}\boldsymbol{D}\boldsymbol{b} + \boldsymbol{v}, \tag{27}$$

where $\boldsymbol{D} \in \mathbb{R}^{N \times N}$ is the DCT matrix and its (i, j) element is given by

$$d_{i,j} = \begin{cases} \sqrt{\dfrac{1}{N}} & (i = 1) \\ \sqrt{\dfrac{2}{N}} \cos\left(\dfrac{\pi}{2N}(i-1)(2j-1)\right) & (i \neq 1) \end{cases} \tag{28}$$

in the simulations. The selection matrix $\boldsymbol{S} \in \mathbb{R}^{M \times N}$ is composed by randomly selecting M rows of the $N \times N$ identity matrix. Figures 8 and 9 show the SER performance for the partial DCT matrix. The distribution of the unknown vector is $\Pr(b_n = 0) = 0.2, \Pr(b_n = -1) = \Pr(b_n = 1) = 0.4$. The problem size is $(N, M) = (1024, 768)$ in Fig. 8 and $(N, M) = (128, 96)$ in Fig. 9. In the figures, "Turbo-CS" denotes the performance of the algorithm based on turbo compressed sensing [26], [27], which has been proposed for the measurement with a partial DFT matrix. Although Turbo-CS achieves the best SER in Fig. 8, it has the error floor in Fig. 9 possibly because the problem size is rather small. In [46], a similar phenomenon can be observed for individually-optimal large MIMO AMP (IO-LAMA) [44],

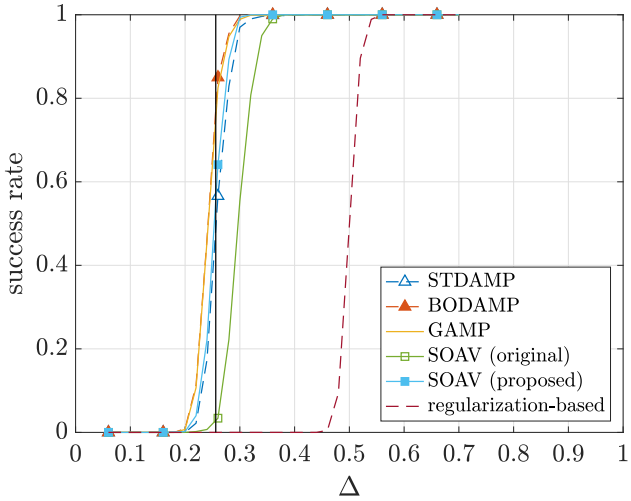

Fig. 10. Success rate in the noise-free case ($\boldsymbol{b} \in \{0,1\}^N$, $\Pr(b_n = 0) = 0.1$, $\Pr(b_n = 1) = 0.9$, and $N = 1000$)

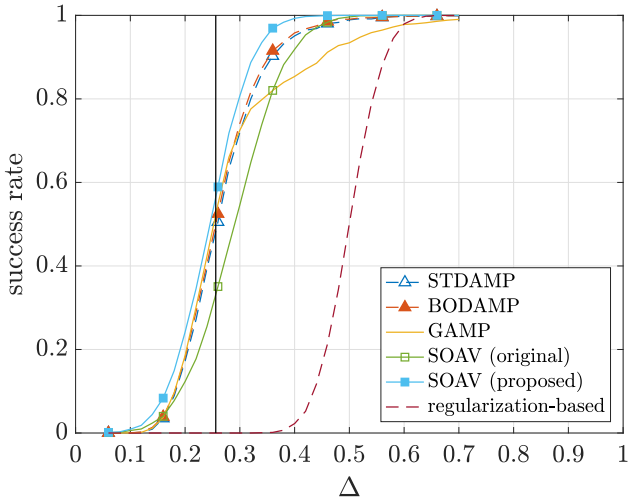

Fig. 11. Success rate in the noise-free case ($\boldsymbol{b} \in \{0,1\}^N$, $\Pr(b_n = 0) = 0.1$, $\Pr(b_n = 1) = 0.9$, and $N = 100$)

which is an AMP-based MIMO signal detection scheme. The SERs at the error floor will depend both on the algorithms and the structure of the measurement matrix. From the figures, we observe that Bayes optimal DAMP and GAMP achieve good performance even if the problem size is not very large when the measurement matrix is a partial DCT matrix. We note again that Bayes optimal DAMP does not require the knowledge of noise variance unlike GAMP.

In Figs. 10 and 11, we empirically evaluate the rate of the success recovery in the sense that $\mathcal{Q}(\boldsymbol{x}^t) = \boldsymbol{b}$ after $t = 300$ iterations. Figure 10 shows the success rate for the binary vector $\boldsymbol{b} \in \{0,1\}^N$ with $N = 1000$. The distribution of the unknown vector is given by $\Pr(b_n = 0) = 0.1$ and $\Pr(b_n = 1) = 0.9$. The measurement matrix is an i.i.d. Gaussian matrix. We consider the noise-free case and hence the SOAV optimization problem is given by

$$\hat{\boldsymbol{b}} = \arg\min_{\boldsymbol{x}\in\mathbb{R}^N} q_1\|\boldsymbol{x}\|_1 + q_2\|\boldsymbol{x} - \boldsymbol{1}\|_1 \quad \text{subject to} \quad \boldsymbol{y} = \boldsymbol{A}\boldsymbol{x}, \tag{29}$$

which is solved by Douglas-Rachford algorithm [18], [47] in the simulation. In the figure, "regularization-based" denotes the regularization-based method [11], which solves (29) with $q_1 = q_2 = 1$. The vertical line corresponds to the value of Δ for $D_{\min} = 1$ obtained from Fig. 1. In the large system limit, the left side of each vertical line is the failure region and the right side is the success region of soft thresholding DAMP in the sense that $\sigma_t^2 \to 0$ ($t \to \infty$). The success rate of soft thresholding DAMP rapidly increases around the vertical line. Moreover, Bayes optimal DAMP, GAMP, and the SOAV optimization with the proposed parameters can achieve slightly better success rates than that of soft thresholding DAMP. Their success rates are also better than those of the SOAV optimization with original coefficients and the regularization-based method. One of possible reasons that the recovery rate is not equal to one in the success region near the boundary is that we restrict the maximum number of iterations as $t = 300$. Another reason will be that the problem size here is finite and not large enough. In Fig. 11, we evaluate the recovery rate for $\boldsymbol{b} \in \{0,1\}^N$ with $N = 100$. Since the problem size is smaller than that in Fig. 10, the performance of the AMP-based algorithms is worse than that of the SOAV optimization with the proposed parameters.

VII. Conclusion

In this paper, we have proposed the algorithm for the discrete-valued vector reconstruction, referred to as DAMP. We have analytically evaluated the asymptotic performance of soft thresholding DAMP and have derived the condition for the perfect reconstruction in the large system limit via state evolution. The optimization algorithm for the parameters of the soft thresholding function enables us to analyze the performance theoretically in some cases. By using the analysis of soft thresholding DAMP, we have also proposed the method to determine the parameters of the SOAV optimization. Moreover, we have provided Bayes optimal DAMP, which gives much smaller MSE compared to soft thresholding DAMP. Via computer simulations, we have shown that DAMP can reconstruct the discrete-valued vector from its underdetermined linear measurements and the empirical performance agrees well with our theoretical results for large-scale problems. For smaller-scale problems, the SOAV optimization with the proposed parameters can achieve better performance than the AMP-based algorithms. We have also shown that Bayes optimal DAMP works well for partial DCT measurement matrices.

Future work includes the extension of the proposed algorithms to the reconstruction of the complex discrete-valued vector, as well as some applications such as signal detection in communication systems and image reconstruction.

Appendix A
Derivation of $\Psi(\sigma^2)$

We firstly rewrite (10) as

$$\Psi(\sigma^2) = \sum_{\ell=1}^{L} p_\ell \Psi_\ell(\sigma^2), \tag{30}$$

where

$$\Psi_\ell(\sigma^2) = \int_{-\infty}^{\infty} \left\{ \eta\left(r_\ell + \frac{\sigma}{\sqrt{\Delta}} z; \frac{\sigma}{\sqrt{\Delta}} \right) - r_\ell \right\}^2 \phi(z) \mathrm{d}z. \tag{31}$$

From (6) and (7), we have

$$\begin{aligned} &\eta\left(r_\ell + \frac{\sigma}{\sqrt{\Delta}} z; \frac{\sigma}{\sqrt{\Delta}} \right) \\ &= \begin{cases} r_\ell + \frac{\sigma}{\sqrt{\Delta}}(z - Q_1) & (z < T_{\ell,1,1}) \\ r_1 & (T_{\ell,1,1} \le z < T_{\ell,1,2}) \\ \quad \vdots & \quad \vdots \\ r_\ell + \frac{\sigma}{\sqrt{\Delta}}(z - Q_k) & (T_{\ell,k-1,k} \le z < T_{\ell,k,k}) \\ r_k & (T_{\ell,k,k} \le z < T_{\ell,k,k+1}) \\ \quad \vdots & \quad \vdots \\ r_\ell + \frac{\sigma}{\sqrt{\Delta}}(z - Q_{L+1}) & (T_{\ell,L,L+1} \le z) \end{cases}, \end{aligned} \tag{32}$$

where

$$T_{\ell,k,k'} = \frac{\sqrt{\Delta}}{\sigma}(-r_\ell + r_k) + Q_{k'}. \tag{33}$$

We thus rewrite $\Psi_\ell(\sigma^2)$ as

$$\begin{aligned} \Psi_\ell(\sigma^2) = &\frac{\sigma^2}{\Delta} \int_{-\infty}^{T_{\ell,1,1}} (z - Q_1)^2 \phi(z) \mathrm{d}z \\ &+ \sum_{k=1}^{L} \int_{T_{\ell,k,k}}^{T_{\ell,k,k+1}} (r_k - r_\ell)^2 \phi(z) \mathrm{d}z \\ &+ \frac{\sigma^2}{\Delta} \sum_{k=2}^{L} \int_{T_{\ell,k-1,k}}^{T_{\ell,k,k}} (z - Q_k)^2 \phi(z) \mathrm{d}z \\ &+ \frac{\sigma^2}{\Delta} \int_{T_{\ell,L,L+1}}^{\infty} (z - Q_{L+1})^2 \phi(z) \mathrm{d}z. \end{aligned} \tag{34}$$

For $a, b, Q \in \mathbb{R}$, we have

$$\begin{aligned} &\int_a^b (z - Q)^2 \phi(z) \mathrm{d}z \\ &= \{ -b\phi(b) + a\phi(a) + \Phi(b) - \Phi(a) \} \\ &\quad - 2Q\{ -\phi(b) + \phi(a) \} + Q^2 \{ \Phi(b) - \Phi(a) \}, \end{aligned} \tag{35}$$

thus

$$\begin{aligned} \Psi_\ell(\sigma^2) = &\sum_{k=1}^{L} (r_k - r_\ell)^2 \{ \Phi(T_{\ell,k,k+1}) - \Phi(T_{\ell,k,k}) \} \\ &+ \frac{\sigma^2}{\Delta} \sum_{k=1}^{L} [\{ -T_{\ell,k,k}\phi(T_{\ell,k,k}) + \Phi(T_{\ell,k,k}) \} \\ &\qquad + 2Q_k\phi(T_{\ell,k,k}) + Q_k^2 \Phi(T_{\ell,k,k})] \\ &+ \frac{\sigma^2}{\Delta} \sum_{k=2}^{L+1} [\{ T_{\ell,k-1,k}\phi(T_{\ell,k-1,k}) - \Phi(T_{\ell,k-1,k}) \} \\ &\qquad - 2Q_k\phi(T_{\ell,k-1,k}) - Q_k^2 \Phi(T_{\ell,k-1,k})] \\ &+ \frac{\sigma^2}{\Delta} \left(1 + Q_{L+1}^2 \right). \end{aligned} \tag{36}$$

Hence, $\Psi(\sigma^2)$ in (30) can be obtained from (36).

Appendix B
Derivation of $\left.\frac{\mathrm{d}\Psi}{\mathrm{d}(\sigma^2)}\right|_{\sigma\downarrow 0}$

From (30), we have

$$\left.\frac{\mathrm{d}\Psi}{\mathrm{d}(\sigma^2)}\right|_{\sigma\downarrow 0} = \sum_{\ell=1}^{L} p_\ell \left.\frac{\mathrm{d}\Psi_\ell}{\mathrm{d}(\sigma^2)}\right|_{\sigma\downarrow 0}. \tag{37}$$

With the derivative of $T_{\ell,k,k'}$ with respect to σ^2

$$T'_{\ell,k,k'} = \frac{\mathrm{d}T_{\ell,k,k'}}{\mathrm{d}(\sigma^2)} \left(= -\frac{\sqrt{\Delta}}{2\sigma^3}(-r_\ell + r_k) \right), \tag{38}$$

the derivative of (36) is given by

$$\begin{aligned} &\frac{\mathrm{d}\Psi_\ell}{\mathrm{d}(\sigma^2)} \\ &= \sum_{k=1}^{L} (r_k - r_\ell)^2 \left\{ T'_{\ell,k,k+1}\phi(T_{\ell,k,k+1}) - T'_{\ell,k,k}\phi(T_{\ell,k,k}) \right\} \\ &\quad + \frac{1}{\Delta} \sum_{k=1}^{L} [\{ -T_{\ell,k,k}\phi(T_{\ell,k,k}) + \Phi(T_{\ell,k,k}) \} \\ &\qquad + 2Q_k\phi(T_{\ell,k,k}) + Q_k^2 \Phi(T_{\ell,k,k})] \\ &\quad + \frac{\sigma^2}{\Delta} \sum_{k=1}^{L} (T_{\ell,k,k} - Q_k)^2 T'_{\ell,k,k}\phi(T_{\ell,k,k}) \\ &\quad + \frac{1}{\Delta} \sum_{k=2}^{L+1} [\{ T_{\ell,k-1,k}\phi(T_{\ell,k-1,k}) - \Phi(T_{\ell,k-1,k}) \} \\ &\qquad - 2Q_k\phi(T_{\ell,k-1,k}) - Q_k^2 \Phi(T_{\ell,k-1,k})] \\ &\quad - \frac{\sigma^2}{\Delta} \sum_{k=2}^{L+1} (T_{\ell,k-1,k} - Q_k)^2 T'_{\ell,k-1,k}\phi(T_{\ell,k-1,k}) \\ &\quad + \frac{1}{\Delta} \left(1 + Q_{L+1}^2 \right) \end{aligned} \tag{39}$$

$$\begin{aligned} &= \frac{1}{\Delta} \sum_{k=1}^{L} [\{ -T_{\ell,k,k}\phi(T_{\ell,k,k}) + \Phi(T_{\ell,k,k}) \} \\ &\qquad + 2Q_k\phi(T_{\ell,k,k}) + Q_k^2 \Phi(T_{\ell,k,k})] \\ &\quad + \frac{1}{\Delta} \sum_{k=2}^{L+1} [\{ T_{\ell,k-1,k}\phi(T_{\ell,k-1,k}) - \Phi(T_{\ell,k-1,k}) \} \\ &\qquad - 2Q_k\phi(T_{\ell,k-1,k}) - Q_k^2 \Phi(T_{\ell,k-1,k})] \\ &\quad + \frac{1}{\Delta} \left(1 + Q_{L+1}^2 \right). \end{aligned} \tag{40}$$

From

$$\lim_{\sigma\downarrow 0} T_{\ell,k,k'} = \begin{cases} \infty & (\ell < k) \\ Q_{k'} & (\ell = k) \\ -\infty & (\ell > k) \end{cases}, \tag{41}$$

we conclude that

$$\begin{aligned}
&\left.\frac{\mathrm{d}\Psi_\ell}{\mathrm{d}(\sigma^2)}\right|_{\sigma\downarrow 0} \\
&= \frac{1}{\Delta}\left[\{-Q_\ell\phi(Q_\ell)+\Phi(Q_\ell)\}+2Q_\ell\phi(Q_\ell)+Q_\ell^2\Phi(Q_\ell)\right] \\
&\quad+\frac{1}{\Delta}\sum_{k=\ell+1}^{L}\left(1+Q_k^2\right) \\
&\quad+\frac{1}{\Delta}\left[\{Q_{\ell+1}\phi(Q_{\ell+1})-\Phi(Q_{\ell+1})\}\right. \\
&\qquad\left.-2Q_{\ell+1}\phi(Q_{\ell+1})-Q_{\ell+1}^2\Phi(Q_{\ell+1})\right] \\
&\quad+\frac{1}{\Delta}\sum_{k=\ell+2}^{L+1}\left(-1-Q_k^2\right) \\
&\quad+\frac{1}{\Delta}\left(1+Q_{L+1}^2\right) \qquad (42)\\
&= \frac{1}{\Delta}\left\{Q_\ell\phi(Q_\ell)-Q_{\ell+1}\phi(Q_{\ell+1})+\left(1+Q_\ell^2\right)\Phi(Q_\ell)\right. \\
&\qquad\left.+\left(1+Q_{\ell+1}^2\right)(1-\Phi(Q_{\ell+1}))\right\}. \qquad (43)
\end{aligned}$$

Hence, $\left.\frac{\mathrm{d}\Psi}{\mathrm{d}(\sigma^2)}\right|_{\sigma\downarrow 0}$ is straightforwardly obtained from (37) and (43) as in (12).

APPENDIX C
PROOF OF THEOREM 1

Since $D(\boldsymbol{Q})$ is a monotonically increasing function of Q_1 and a monotonically decreasing function of Q_{L+1}, their optimal values are $Q_1^{\mathrm{opt}}=-\infty$ and $Q_{L+1}^{\mathrm{opt}}=\infty$, respectively. Thus, the optimization problem (13) can be reduced to

$$\begin{aligned}
D_{\min} = &\min_{Q_2,\ldots,Q_L}\tilde{D}(Q_2,\ldots,Q_L) \\
&\text{subject to } Q_2\le\cdots\le Q_L, \qquad (44)
\end{aligned}$$

where

$$\begin{aligned}
&\tilde{D}(Q_2,\ldots,Q_L) \\
&:= \left.\frac{\Delta}{2}D(\boldsymbol{Q})\right|_{Q_1=-\infty,Q_{L+1}=\infty} \qquad (45)\\
&= \frac{1}{2}\sum_{\ell=2}^{L}\left[p_{\ell-1}\left\{-Q_\ell\phi(Q_\ell)+\left(1+Q_\ell^2\right)(1-\Phi(Q_\ell))\right\}\right. \\
&\qquad\left.+p_\ell\left\{Q_\ell\phi(Q_\ell)+\left(1+Q_\ell^2\right)\Phi(Q_\ell)\right\}\right]. \qquad (46)
\end{aligned}$$

It is sufficient to confirm that $\tilde{D}(Q_2\ldots,Q_L)$ is strictly convex and $Q_2^{\mathrm{opt}},\ldots,Q_L^{\mathrm{opt}}$ obtained by Algorithm 2 satisfies Karush-Kuhn-Tucker (KKT) conditions of (44).

A. Strict Convexity of $\tilde{D}(Q_2\ldots,Q_L)$

To prove the strict convexity of $\tilde{D}(Q_2\ldots,Q_L)$, we show that the Hessian $\nabla^2\tilde{D}$ is positive definite. The partial derivative of $\tilde{D}(Q_2\ldots,Q_L)$ with respect to Q_ℓ $(\ell=2,\ldots,L)$ is given by

$$\begin{aligned}
\frac{\partial\tilde{D}}{\partial Q_\ell} = &p_{\ell-1}\left\{-\phi(Q_\ell)+Q_\ell(1-\Phi(Q_\ell))\right\} \\
&+p_\ell\left\{\phi(Q_\ell)+Q_\ell\Phi(Q_\ell)\right\}. \qquad (47)
\end{aligned}$$

The second-order partial derivative can be written as

$$\frac{\partial^2\tilde{D}}{\partial Q_\ell^2} = p_{\ell-1}(1-\Phi(Q_\ell))+p_\ell\Phi(Q_\ell)>0, \qquad (48)$$

and

$$\frac{\partial^2\tilde{D}}{\partial Q_\ell\partial Q_{\ell'}} = 0\ (\ell\ne\ell'). \qquad (49)$$

From (48) and (49), the Hessian $\nabla^2\tilde{D} = \mathrm{diag}\left(\frac{\partial^2\tilde{D}}{\partial Q_2^2},\ldots,\frac{\partial^2\tilde{D}}{\partial Q_L^2}\right)$ is positive definite and hence $\tilde{D}(Q_2,\ldots,Q_L)$ is a strictly convex function of $Q_2,\ldots,Q_L$.

B. KKT Conditions

Next, we prove that $Q_2^{\mathrm{opt}},\ldots,Q_L^{\mathrm{opt}}$ satisfies the KKT conditions of (44). We define the Lagrange function as

$$\mathcal{L}(Q_2,\ldots,Q_L)=\tilde{D}(Q_2,\ldots,Q_L)+\sum_{\ell=2}^{L-1}\mu_\ell(Q_\ell-Q_{\ell+1}), \qquad (50)$$

where $\mu_2,\ldots,\mu_{L-1}$ are the KKT multipliers. Since the partial derivatives of $\tilde{D}(Q_2,\ldots,Q_L)$ are obtained as in (47), the KKT conditions can be written with $F_\ell(Q)$ $(\ell=2,\ldots,L)$ defined in Algorithm 2.

KKT conditions of (44)

1) $F_2(Q_2)+\mu_2=0$,
   $F_\ell(Q_\ell)-\mu_{\ell-1}+\mu_\ell=0$ $(\ell=3,\ldots,L-1)$,
   $F_L(Q_L)-\mu_{L-1}=0$.
2) $Q_\ell-Q_{\ell+1}\le 0$ $(\ell=2,\ldots,L-1)$.
3) $\mu_\ell\ge 0$ $(\ell=2,\ldots,L-1)$.
4) $\mu_\ell(Q_\ell-Q_{\ell+1})=0$ $(\ell=2,\ldots,L-1)$.

Before the investigation of the KKT conditions, we confirm that the equations $G_\ell(Q)=0$ and $\sum_{k=j}^{\ell-1}F_k(Q)=0$ have a unique solution and $\hat{Q}(\cdot)$ in Algorithm 2 can be defined properly. For $\ell=2,\ldots,L$, we have $\lim_{Q\to-\infty}F_\ell(Q)=-\infty$, $\lim_{Q\to\infty}F_\ell(Q)=\infty$, and

$$\frac{\mathrm{d}F_\ell}{\mathrm{d}Q} = p_{\ell-1}(1-\Phi(Q))+p_\ell\Phi(Q)>0, \qquad (51)$$

which show that each $F_\ell(Q)$ is a strictly increasing function with the range $\mathbb{R}$. Since $G_\ell(Q)$ and $\sum_{k=j}^{\ell-1}F_k(Q)$ are sum of some $F_\ell(Q)$ $(\ell=2,\ldots,L)$, they are also strictly increasing functions with the range $\mathbb{R}$ and the solutions of $G_\ell(Q)=0$ and $\sum_{k=j}^{\ell-1}F_k(Q)=0$ are unique.

We then prove that $Q_2^{\mathrm{opt}},\ldots,Q_L^{\mathrm{opt}}$ obtained by Algorithm 2 and $\mu_\ell^{\mathrm{opt}}:=G_{\ell+1}\left(Q_{\ell+1}^{\mathrm{opt}}\right)$ $(\ell=2,\ldots,L-1)$ satisfy the KKT conditions, i.e.,

$$\begin{aligned}
F_2\left(Q_2^{\mathrm{opt}}\right)+\mu_2^{\mathrm{opt}} &= 0, &(52)\\
F_\ell\left(Q_\ell^{\mathrm{opt}}\right)-\mu_{\ell-1}^{\mathrm{opt}}+\mu_\ell^{\mathrm{opt}} &= 0\ (\ell=3,\ldots,L-1), &(53)\\
F_L\left(Q_L^{\mathrm{opt}}\right)-\mu_{L-1}^{\mathrm{opt}} &= 0, &(54)\\
Q_\ell^{\mathrm{opt}}-Q_{\ell+1}^{\mathrm{opt}} &\le 0\ (\ell=2,\ldots,L-1), &(55)\\
\mu_\ell^{\mathrm{opt}} &\ge 0\ (\ell=2,\ldots,L-1), &(56)\\
\mu_\ell^{\mathrm{opt}}\left(Q_\ell^{\mathrm{opt}}-Q_{\ell+1}^{\mathrm{opt}}\right) &= 0\ (\ell=2,\ldots,L-1). &(57)
\end{aligned}$$

In the following proofs of (52)–(57), we denote the condition $\hat{Q}(G_\ell(Q)) > \max_{j=2,\dots,\ell-1} \hat{Q}\left(\sum_{k=j}^{\ell-1} F_k(Q)\right)$ in the line 8 of Algorithm 2 by H_ℓ.

1) proof of (52)–(54)*:* From the definition of $G_\ell(Q)$, we have $G_\ell\left(Q_\ell^{\text{opt}}\right) = F_\ell\left(Q_\ell^{\text{opt}}\right) + G_{\ell+1}\left(Q_{\ell+1}^{\text{opt}}\right)$ for $\ell = 3, \dots, L-1$. We thus obtain

$$\begin{aligned} &F_\ell\left(Q_\ell^{\text{opt}}\right) - \mu_{\ell-1}^{\text{opt}} + \mu_\ell^{\text{opt}} \\ &= F_\ell\left(Q_\ell^{\text{opt}}\right) - G_\ell\left(Q_\ell^{\text{opt}}\right) + G_{\ell+1}\left(Q_{\ell+1}^{\text{opt}}\right) \qquad (58) \\ &= 0. \qquad (59) \end{aligned}$$

Similarly, we have $F_2\left(Q_2^{\text{opt}}\right) + \mu_2^{\text{opt}} = F_2\left(Q_2^{\text{opt}}\right) + G_3\left(Q_3^{\text{opt}}\right) = G_2\left(Q_2^{\text{opt}}\right) = G_2\left(\hat{Q}(G_2(Q))\right) = 0$ and $F_L\left(Q_L^{\text{opt}}\right) - \mu_{L-1}^{\text{opt}} = F_L\left(Q_L^{\text{opt}}\right) - G_L\left(Q_L^{\text{opt}}\right) = 0$ because $G_L(Q) = F_L(Q)$.

2) proof of (55)*:* We firstly consider the case where the condition $H_{\ell+1}$ is satisfied. In this case, $Q_{\ell+1}^{\text{opt}}$ is determined as $Q_{\ell+1}^{\text{opt}} = \hat{Q}\left(G_{\ell+1}(Q)\right)$. We define ℓ' $(< \ell)$ as the maximum index that $H_{\ell'}$ is true, i.e., the conditions $H_\ell, H_{\ell-1}, \dots, H_{\ell'+1}$ are not satisfied and the condition $H_{\ell'}$ is satisfied. By using Algorithm 2, we can obtain $G_{\ell'}(Q) = \sum_{k=\ell'}^{\ell} F_k(Q)$ and $Q_\ell^{\text{opt}} = Q_{\ell-1}^{\text{opt}} = \cdots = Q_{\ell'}^{\text{opt}} = \hat{Q}\left(G_{\ell'}(Q)\right)$. We thus have $Q_{\ell+1}^{\text{opt}} = \hat{Q}\left(G_{\ell+1}(Q)\right) > \hat{Q}\left(\sum_{k=\ell'}^{\ell} F_k(Q)\right) = \hat{Q}\left(G_{\ell'}(Q)\right) = Q_\ell^{\text{opt}}$ and hence $Q_\ell^{\text{opt}} - Q_{\ell+1}^{\text{opt}} \le 0$.

If the condition $H_{\ell+1}$ is not satisfied and $Q_{\ell+1}^{\text{opt}} = Q_\ell^{\text{opt}}$, we also have $Q_\ell^{\text{opt}} - Q_{\ell+1}^{\text{opt}} \le 0$.

3) proof of (56)*:* If the condition $H_{\ell+1}$ is satisfied, $\mu_\ell^{\text{opt}} = G_{\ell+1}\left(Q_{\ell+1}^{\text{opt}}\right) = G_{\ell+1}\left(\hat{Q}(G_{\ell+1}(Q))\right) = 0$ and hence $\mu_\ell^{\text{opt}} \ge 0$ holds.

Next, we assume that the condition $H_{\ell+1}$ is not satisfied. In this case, we have

$$\hat{Q}\left(G_{\ell+1}(Q)\right) \le \max_{j=2,\dots,\ell} \hat{Q}\left(\sum_{k=j}^{\ell} F_k(Q)\right). \qquad (60)$$

We define ℓ' $(< \ell+1)$ as the maximum index that $H_{\ell'}$ is true, i.e., the conditions $H_\ell, H_{\ell-1}, \dots, H_{\ell'+1}$ are not satisfied and the condition $H_{\ell'}$ is satisfied. We can obtain

$$\hat{Q}\left(G_{\ell'}(Q)\right) > \max_{j=2,\dots,\ell'-1} \hat{Q}\left(\sum_{k=j}^{\ell'-1} F_k(Q)\right), \qquad (61)$$

$$G_{\ell'}(Q) = G_{\ell+1}(Q) + \sum_{k=\ell'}^{\ell} F_k(Q), \qquad (62)$$

and $Q_{\ell+1}^{\text{opt}} = Q_\ell^{\text{opt}} = \cdots = Q_{\ell'}^{\text{opt}} = \hat{Q}\left(G_{\ell'}(Q)\right)$. In what follows, we often use the following lemma.

Lemma 1. For strictly increasing functions $f(Q)$ and $g(Q)$ with the range $\mathbb{R}$, we have

$$\begin{aligned} &\hat{Q}\left(f(Q)\right) < \hat{Q}\left(g(Q)\right) \\ &\iff \hat{Q}\left(f(Q)\right) < \hat{Q}\left(f(Q) + g(Q)\right) < \hat{Q}\left(g(Q)\right). \qquad (63) \end{aligned}$$

The proposition obtained by replacing all of $<$ with $\le$ also holds.

To prove $\mu_\ell^{\text{opt}} \ge 0$, we will show that

$$\hat{Q}\left(G_{\ell+1}(Q)\right) \le \hat{Q}\left(\sum_{k=\ell'}^{\ell} F_k(Q)\right), \qquad (64)$$

which results in $\hat{Q}\left(G_{\ell+1}(Q)\right) \le \hat{Q}\left(G_{\ell'}(Q)\right)$ from (62) and Lemma 1. If $\hat{Q}\left(G_{\ell+1}(Q)\right) \le \hat{Q}\left(G_{\ell'}(Q)\right)$ holds, we can obtain $\mu_\ell^{\text{opt}} \ge 0$ as $\mu_\ell^{\text{opt}} = G_{\ell+1}\left(Q_{\ell+1}^{\text{opt}}\right) = G_{\ell+1}\left(Q_{\ell'}^{\text{opt}}\right) = G_{\ell+1}\left(\hat{Q}\left(G_{\ell'}(Q)\right)\right) \ge G_{\ell+1}\left(\hat{Q}\left(G_{\ell+1}(Q)\right)\right) = 0$.

To show (64), we provide the proof by contradiction with the assumption

$$\hat{Q}\left(G_{\ell+1}(Q)\right) > \hat{Q}\left(\sum_{k=\ell'}^{\ell} F_k(Q)\right). \qquad (65)$$

From (62), (65) and Lemma 1, we have

$$\hat{Q}\left(\sum_{k=\ell'}^{\ell} F_k(Q)\right) < \hat{Q}\left(G_{\ell'}(Q)\right) < \hat{Q}\left(G_{\ell+1}(Q)\right). \qquad (66)$$

It follows from (61) and (66) that

$$\max_{j=2,\dots,\ell'} \hat{Q}\left(\sum_{k=j}^{\ell} F_k(Q)\right) < \hat{Q}\left(G_{\ell'}(Q)\right) < \hat{Q}\left(G_{\ell+1}(Q)\right). \qquad (67)$$

From (60) and (67), we can obtain

$$\hat{Q}\left(G_{\ell+1}(Q)\right) \le \max_{j=\ell'+1,\dots,\ell} \hat{Q}\left(\sum_{k=j}^{\ell} F_k(Q)\right). \qquad (68)$$

We define ℓ_1 as $\ell_1 = \arg\max_{j=\ell'+1,\dots,\ell} \hat{Q}\left(\sum_{k=j}^{\ell} F_k(Q)\right)$, which results in

$$\hat{Q}\left(G_{\ell+1}(Q)\right) \le \hat{Q}\left(\sum_{k=\ell_1}^{\ell} F_k(Q)\right). \qquad (69)$$

Since $\ell' + 1 \le \ell_1 \le \ell$, the conditions $H_\ell, \dots, H_{\ell_1}$ are not satisfied and hence we have

$$\hat{Q}(G_{\ell_1}(Q)) \le \max_{j=2,\dots,\ell_1-1} \hat{Q}\left(\sum_{k=j}^{\ell_1-1} F_k(Q)\right), \qquad (70)$$

$$G_{\ell_1}(Q) = G_{\ell+1}(Q) + \sum_{k=\ell_1}^{\ell} F_k(Q). \qquad (71)$$

Lemma 1, (69), and (71) give

$$\hat{Q}\left(G_{\ell+1}(Q)\right) \le \hat{Q}\left(G_{\ell_1}(Q)\right) \le \hat{Q}\left(\sum_{k=\ell_1}^{\ell} F_k(Q)\right). \qquad (72)$$

From (67) and (72), we have

$$\hat{Q}\left(G_{\ell'}(Q)\right) < \hat{Q}\left(G_{\ell+1}(Q)\right) \le \hat{Q}\left(G_{\ell_1}(Q)\right). \qquad (73)$$

With a similar approach to (71), we can also obtain

$$G_{\ell'}(Q) = G_{\ell_1}(Q) + \sum_{k=\ell'}^{\ell_1-1} F_k(Q) \qquad (74)$$

and

$$\hat{Q}\left(\sum_{k=\ell'}^{\ell_1-1} F_k(Q)\right) \leq \hat{Q}\left(G_{\ell'}(Q)\right) < \hat{Q}\left(G_{\ell_1}(Q)\right). \quad (75)$$

It follows from (61) and (75) that

$$\max_{j=2,\ldots,\ell'} \hat{Q}\left(\sum_{k=j}^{\ell_1-1} F_k(Q)\right) < \hat{Q}\left(G_{\ell_1}(Q)\right). \quad (76)$$

If $\ell_1 = \ell' + 1$, (76) contradicts (70) and hence we can conclude (64) and $\mu_\ell^{\text{opt}} \geq 0$. Otherwise $\ell_1 > \ell' + 1$, and in this case combining (70) and (76) gives

$$\hat{Q}(G_{\ell_1}(Q)) \leq \max_{j=\ell'+1,\ldots,\ell_1-1} \hat{Q}\left(\sum_{k=j}^{\ell_1-1} F_k(Q)\right). \quad (77)$$

We then define ℓ_2 as $\ell_2 = \arg\max_{j=\ell'+1,\ldots,\ell_1-1} \hat{Q}\left(\sum_{k=j}^{\ell_1-1} F_k(Q)\right)$. Here, note that $\ell'+1 \leq \ell_2 < \ell_1 < \ell+1$. By repeating the same manner, we have a sequence $\ell_1, \ell_2, \ldots, \ell_i$ satisfying $\ell'+i-1 \leq \ell_i < \ell_{i-1} < \cdots < \ell_1 < \ell + 1$. Since $\{\ell' + i - 1\}_{i=1,\ldots}$ is monotonically increasing and $\{\ell_i\}_{i=1,\ldots}$ is monotonically decreasing, there exists $\tilde{i}$ satisfying $\ell' + \tilde{i} - 1 = \ell_{\tilde{i}} < \ell_{\tilde{i}-1} < \cdots < \ell_1 < \ell + 1$. Moreover, similar to (76), we have

$$\hat{Q}\left(G_{\ell_{\tilde{i}}}(Q)\right) > \max_{j=2,\ldots,\ell'+\tilde{i}-2} \hat{Q}\left(\sum_{k=j}^{\ell_{\tilde{i}}-1} F_k(Q)\right) \quad (78)$$

$$= \max_{j=2,\ldots,\ell_{\tilde{i}}-1} \hat{Q}\left(\sum_{k=j}^{\ell_{\tilde{i}}-1} F_k(Q)\right). \quad (79)$$

However, (79) contradicts the fact that ℓ' $(< \ell + 1)$ is the maximum index of $H_{\ell'}$ being true because $\ell_{\tilde{i}} > \ell'$. We thus conclude (64) and $\mu_\ell^{\text{opt}} \geq 0$.

4) proof of (57)*:* If the condition $H_{\ell+1}$ is satisfied and $Q_{\ell+1}^{\text{opt}}$ is determined as $Q_{\ell+1}^{\text{opt}} = \hat{Q}\left(G_{\ell+1}(Q)\right)$, $\mu_\ell^{\text{opt}} = G_{\ell+1}\left(Q_{\ell+1}^{\text{opt}}\right) = 0$ and hence $\mu_\ell^{\text{opt}}\left(Q_\ell^{\text{opt}} - Q_{\ell+1}^{\text{opt}}\right) = 0$ holds. Otherwise, $Q_{\ell+1}^{\text{opt}} = Q_\ell^{\text{opt}}$ and hence $\mu_\ell^{\text{opt}}\left(Q_\ell^{\text{opt}} - Q_{\ell+1}^{\text{opt}}\right) = 0$ also holds.

APPENDIX D
DERIVATION OF $\frac{\mathrm{d}^2\Psi}{\mathrm{d}(\sigma^2)^2}$

From (40), the second derivative of $\Psi_\ell(\sigma^2)$ is given by

$$\begin{aligned}
&\frac{\mathrm{d}^2\Psi_\ell}{\mathrm{d}(\sigma^2)^2} \\
&= \frac{1}{\Delta}\sum_{k=1}^{L}\left\{T_{\ell,k,k}^2 T'_{\ell,k,k}\phi\left(T_{\ell,k,k}\right) - 2Q_k T_{\ell,k,k} T'_{\ell,k,k}\phi\left(T_{\ell,k,k}\right)\right. \\
&\qquad \left. + Q_k^2 T'_{\ell,k,k}\phi\left(T_{\ell,k,k}\right)\right\} \\
&\quad - \frac{1}{\Delta}\sum_{k=2}^{L+1}\left\{T_{\ell,k-1,k}^2 T'_{\ell,k-1,k}\phi\left(T_{\ell,k-1,k}\right)\right. \\
&\qquad - 2Q_k T_{\ell,k-1,k} T'_{\ell,k-1,k}\phi\left(T_{\ell,k-1,k}\right) \\
&\qquad \left. + Q_k^2 T'_{\ell,k-1,k}\phi\left(T_{\ell,k-1,k}\right)\right\} \quad (80)
\end{aligned}$$

$$\begin{aligned}
&= \frac{1}{\Delta}\sum_{k=1}^{L}\left(T_{\ell,k,k} - Q_k\right)^2 T'_{\ell,k,k}\phi\left(T_{\ell,k,k}\right) \\
&\quad - \frac{1}{\Delta}\sum_{k=2}^{L+1}\left(T_{\ell,k-1,k} - Q_k\right)^2 T'_{\ell,k-1,k}\phi\left(T_{\ell,k-1,k}\right) \quad (81)
\end{aligned}$$

$$= \frac{\sqrt{\Delta}}{2\sigma^5}\sum_{k=1}^{L}\left(-r_\ell + r_k\right)^3\left\{-\phi\left(T_{\ell,k,k}\right) + \phi\left(T_{\ell,k,k+1}\right)\right\}, \quad (82)$$

which results in (15).

REFERENCES

[1] S. Verdú, *Multiuser Detection*. Cambridge University Press, 1998.
[2] Y. Kabashima, "A CDMA multiuser detection algorithm on the basis of belief propagation," *J. Phys. A*, vol. 36, no. 43, pp. 11 111–11 121, Oct. 2003.
[3] H. Zhu and G. B. Giannakis, "Exploiting sparse user activity in multiuser detection," *IEEE Trans. Commun.*, vol. 59, no. 2, pp. 454–465, Feb. 2011.
[4] H. Sasahara, K. Hayashi, and M. Nagahara, "Multiuser detection based on MAP estimation with sum-of-absolute-values relaxation," *IEEE Trans. Signal Process.*, vol. 65, no. 21, pp. 5621–5634, Nov. 2017.
[5] K. K. Wong, A. Paulraj, and R. D. Murch, "Efficient high-performance decoding for overloaded MIMO antenna systems," *IEEE Trans. Wireless Commun.*, vol. 6, no. 5, pp. 1833–1843, May 2007.
[6] T. Datta, N. Srinidhi, A. Chockalingam, and B. S. Rajan, "Low-complexity near-optimal signal detection in underdetermined large-MIMO systems," in *Proc. IEEE NCC*, Feb. 2012.
[7] R. Hayakawa and K. Hayashi, "Convex optimization-based signal detection for massive overloaded MIMO systems," *IEEE Trans. Wireless Commun.*, vol. 16, no. 11, pp. 7080–7091, Nov. 2017.
[8] J. E. Mazo, "Faster-than-Nyquist signaling," *Bell System Tech. J.*, vol. 54, no. 8, pp. 1451–1462, Oct. 1975.
[9] H. Sasahara, K. Hayashi, and M. Nagahara, "Symbol detection for faster-than-Nyquist signaling by sum-of-absolute-values optimization," *IEEE Signal Process. Lett.*, vol. 23, no. 12, pp. 1853–1857, Dec. 2016.
[10] A. Tuysuzoglu, W. C. Karl, I. Stojanovic, D. Castañòn, and M. S. Ünlü, "Graph-cut based discrete-valued image reconstruction," *IEEE Trans. Image Process.*, vol. 24, no. 5, pp. 1614–1627, May 2015.
[11] A. Aïssa-El-Bey, D. Pastor, S. M. A. Sbaï, and Y. Fadlallah, "Sparsity-based recovery of finite alphabet solutions to underdetermined linear systems," *IEEE Trans. Inf. Theory*, vol. 61, no. 4, pp. 2008–2018, Apr. 2015.
[12] D. L. Donoho, "Compressed sensing," *IEEE Trans. Inf. Theory*, vol. 52, no. 4, pp. 1289–1306, Apr. 2006.
[13] K. Hayashi, M. Nagahara, and T. Tanaka, "A user's guide to compressed sensing for communications systems," *IEICE Trans. Commun.*, vol. E96-B, no. 3, pp. 685–712, Mar. 2013.
[14] S. Boyd and L. Vandenberghe, *Convex Optimization*. Cambridge University Press, 2004.
[15] P. H. Tan, L. K. Rasmussen, and T. J. Lim, "Constrained maximum-likelihood detection in CDMA," *IEEE Trans. Commun.*, vol. 49, no. 1, pp. 142–153, Jan. 2001.
[16] C. Thrampoulidis, E. Abbasi, W. Xu, and B. Hassibi, "BER analysis of the box relaxation for BPSK signal recovery," in *Proc. IEEE ICASSP*, Mar. 2016.
[17] M. Nagahara, "Discrete signal reconstruction by sum of absolute values," *IEEE Signal Process. Lett.*, vol. 22, no. 10, pp. 1575–1579, Oct. 2015.
[18] P. L. Combettes and J.-C. Pesquet, "Proximal splitting methods in signal processing," in *Fixed-point algorithms for inverse problems in science and engineering*. Springer, 2011.
[19] R. Hayakawa and K. Hayashi, "Discreteness-aware AMP for reconstruction of symmetrically distributed discrete variables," in *Proc. IEEE SPAWC*, Jul. 2017.
[20] ——, "Binary vector reconstruction via discreteness-aware approximate message passing," in *Proc. APSIPA ASC*, Dec. 2017.
[21] D. L. Donoho, A. Maleki, and A. Montanari, "Message-passing algorithms for compressed sensing," *Proc. Nat. Acad. Sci.*, vol. 106, no. 45, pp. 18 914–18 919, Nov. 2009.
[22] ——, "Message passing algorithms for compressed sensing: I. motivation and construction," in *Proc. IEEE Inf. Theory Workshop*, Jan. 2010.
[23] J. Pearl, *Probabilistic Reasoning in Intelligent Systems: Networks of Plausible Inference*. Morgan Kaufmann Publishers Inc., 1988.

[24] F. R. Kschischang, B. J. Frey, and H. A. Loeliger, "Factor graphs and the sum-product algorithm," *IEEE Trans. Inf. Theory*, vol. 47, no. 2, pp. 498–519, Feb. 2001.
[25] M. Bayati and A. Montanari, "The dynamics of message passing on dense graphs, with applications to compressed sensing," *IEEE Trans. Inf. Theory*, vol. 57, no. 2, pp. 764–785, Feb. 2011.
[26] J. Ma, X. Yuan, and L. Ping, "Turbo compressed sensing with partial DFT sensing matrix," *IEEE Signal Process. Lett.*, vol. 22, no. 2, pp. 158–161, Feb. 2015.
[27] Z. Xue, J. Ma, and X. Yuan, "Denoising-based turbo compressed sensing," *IEEE Access*, vol. 5, pp. 7193–7204, 2017.
[28] D. L. Donoho, A. Maleki, and A. Montanari, "Message passing algorithms for compressed sensing: II. analysis and validation," in *Proc. IEEE Inf. Theory Workshop*, Jan. 2010.
[29] ——, "The noise-sensitivity phase transition in compressed sensing," *IEEE Trans. Inf. Theory*, vol. 57, no. 10, pp. 6920–6941, Oct. 2011.
[30] D. Donoho and A. Montanari, "High dimensional robust M-estimation: Asymptotic variance via approximate message passing," *Probability Theory and Related Fields*, vol. 166, no. 3, pp. 935–969, Dec. 2016.
[31] M. Advani and S. Ganguli, "An equivalence between high dimensional bayes optimal inference and M-estimation," in *Proc. NIPS*, Dec. 2016.
[32] R. Hayakawa and K. Hayashi, "Error recovery for massive MIMO signal detection via reconstruction of discrete-valued sparse vector," *IEICE Trans. Fundamentals*, vol. E100-B, no. 12, pp. 2671–2679, Dec. 2017.
[33] Z. Tian, G. Leus, and V. Lottici, "Detection of sparse signals under finite-alphabet constraints," in *Proc. IEEE ICASSP*, Apr. 2009.
[34] A. Müller, D. Sejdinovic, and R. Piechocki, "Approximate message passing under finite alphabet constraints," in *Proc. IEEE ICASSP*, Mar. 2012.
[35] B. Shim, S. Kwon, and B. Song, "Sparse detection with integer constraint using multipath matching pursuit," *IEEE Commun. Lett.*, vol. 18, no. 10, pp. 1851–1854, Oct. 2014.
[36] S. Sparrer and R. F. H. Fischer, "Enhanced iterative hard thresholding for the estimation of discrete-valued sparse signals," in *Proc. EUSIPCO*, Aug. 2016.
[37] N. M. B. Souto and H. A. Lopes, "Efficient recovery algorithm for discrete valued sparse signals using an ADMM approach," *IEEE Access*, vol. 5, pp. 19 562–19 569, 2017.
[38] C. Jeon, A. Maleki, and C. Studer, "On the performance of mismatched data detection in large MIMO systems," in *Proc. IEEE ISIT*, Jul. 2016.
[39] A. Beck and M. Teboulle, "A fast iterative shrinkage-thresholding algorithm for linear inverse problems," *SIAM J. Imag. Sci.*, vol. 2, no. 1, pp. 183–202, Mar. 2009.
[40] K. Mimura, "On introducing damping to bayes optimal approximate message passing for compressed sensing," in *Proc. APSIPA ASC*, Dec. 2015.
[41] A. Montanari and D. Tse, "Analysis of belief propagation for non-linear problems: The example of CDMA (or: How to prove Tanaka's formula)," in *Proc. IEEE Inf. Theory Workshop*, Mar. 2006.
[42] S. Rangan, "Generalized approximate message passing for estimation with random linear mixing," in *Proc. IEEE ISIT*, Jul./Aug. 2011.
[43] S. Rangan, P. Schniter, E. Riegler, A. K. Fletcher, and V. Cevher, "Fixed points of generalized approximate message passing with arbitrary matrices," *IEEE Trans. Inf. Theory*, vol. 62, no. 12, pp. 7464–7474, Dec. 2016.
[44] C. Jeon, R. Ghods, A. Maleki, and C. Studer, "Optimality of large MIMO detection via approximate message passing," in *Proc. IEEE ISIT*, Jun. 2015.
[45] H. Shin and J. H. Lee, "Capacity of multiple-antenna fading channels: spatial fading correlation, double scattering, and keyhole," *IEEE Trans. Inf. Theory*, vol. 49, no. 10, pp. 2636–2647, Oct. 2003.
[46] J. W. Choi and B. Shim, "Detection of large-scale wireless systems via sparse error recovery," *IEEE Trans. Signal Process.*, vol. 65, no. 22, pp. 6038–6052, Nov. 2017.
[47] P. L. Lions and B. Mercier, "Splitting algorithms for the sum of two nonlinear operators," *SIAM J. Numer. Anal.*, vol. 16, no. 6, pp. 964–979, 1979.

PLACE PHOTO HERE

Ryo Hayakawa received the bachelor's degree in engineering and the master's degree in informatics from Kyoto University, Kyoto, Japan, in 2015 and 2017, respectively. He is currently pursuing the Ph.D. degree with the Department of Systems Science, Graduate School of Informatics, Kyoto University. He is a Research Fellow (DC1) of the Japan Society for the Promotion of Science (JSPS). He received the Telecom System Technology Student Award from the Telecommunications Advancement Foundation in 2018. His research interests include signal processing and wireless communication. He is a student member of IEICE.

PLACE PHOTO HERE

Kazunori Hayashi is currently a Professor at Graduate School of Engineering, Osaka City University. He received the B.E., M.E., and Ph.D. degrees in communication engineering from Osaka University, Osaka, Japan, in 1997, 1999 and 2002, respectively. He was an Assistant Professor from 2002 to 2007, and an Associate Professor from 2007 to 2017 at Graduate School of Informatics, Kyoto University. His research interests include statistical signal processing for communication systems. He received the ICF Research Award from the KDDI Foundation in 2008, the IEEE Globecom 2009 Best Paper Award, the IEICE Communications Society Best Paper Award in 2010, the WPMC'11 Best Paper Award, the Telecommunications Advancement Foundation Award in 2012, and the IEICE Communications Society Best Tutorial Paper Award in 2013. He is a member of IEICE, APSIPA, and ISCIE.